NATIONAL ENERGY TECHNOLOGY LABORATORY

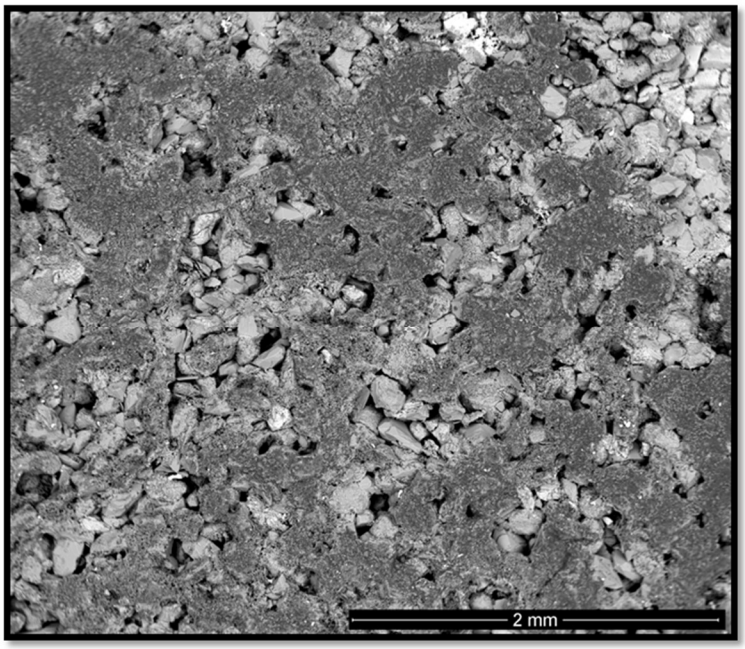

Characterization of the Oriskany and Berea Sandstones: Evaluating Biogeochemical Reactions of Potential Sandstone–Hydraulic Fracturing Fluid Interaction

22 November 2016

U.S. DEPARTMENT OF ENERGY | NATIONAL ENERGY TECHNOLOGY LABORATORY

Office of Fossil Energy

NETL-TRS-13-2016

Disclaimer

Cover Illustration: The cover depicts the top of the inflow sample of Berea sandstone after guar gum flow-though. The Berea sandstone is coated by a thin (<10 μm thick) layer of guar gum.

Suggested Citation: Mordensky, S. P.; Rabjohns, K.; Harris, A.; Lieuallen, A. E.; Verba, C. *Characterization of the Oriskany and Berea Sandstones: Evaluating Biogeochemical Reactions of Potential Sandstone–Hydraulic Fracturing Fluid Interaction*; NETL-TRS-13-2016; NETL Technical Report Series; U.S. Department of Energy, National Energy Technology Laboratory: Albany, OR, 2016; p 48.

An electronic version of this report can be found at:

http://www.netl.doe.gov/research/on-site-research/publications/featured-technical-reports

https://edx.netl.doe.gov/ucr

Characterization of the Oriskany and Berea Sandstones: Evaluating Biogeochemical Reactions of Potential Sandstone–Hydraulic Fracturing Fluid Interaction

Stanley P. Mordensky[1,2], Kelley Rabjohns[1,2], Aubrey Harris[1,3], A. Erin Lieuallen[1,2], Circe Verba[2]

[1] Oak Ridge Institute for Science and Education, MC-100-44, Oak Ridge, TN 37831

[2] U.S. Department of Energy, National Energy Technology Laboratory, 1450 Queen Avenue SW, Albany, OR 97321

[3] U.S. Department of Energy, National Energy Technology Laboratory, 3610 Collins Ferry Road, Morgantown, WV 26507

NETL-TRS-13-2016

22 November 2016

NETL Contacts:

Daniel Soeder, Principal Investigator

Alexandra Hakala, Technical Portfolio Lead

Cynthia Powell, Executive Director, Research & Innovation Center

This page intentionally left blank.

Table of Contents

This page intentionally left blank.

List of Figures

List of Tables

Acronyms, Abbreviations, and Symbols

Term	Description
1,5 Pentanediol	$HOCH_2CH_2CH_2CH_2CH_2OH$
5-Hydroxypentanal	$C_5H_{10}O_2$
Acetate	CH_3COO
Anhydrite	$CaSO_4$
Apatite	$Ca_{10}(PO_4)_6(OH,F,Cl)_2$
Barite	$BaSO_4$
Bicarbonate	HCO_3-
BSE	Back-scattered electrons
Calcite	$CaCO_3$
Carbogen	HC
Celestite	$SrSO_4$
Chlorite	$(Mg,Fe^{2+},Mn,Al)_{12}((Si,Al)_8O_{20})(OH)_{16}$
Chromite	$FeCr_2O_4$
Dolomite	$CaMg(CO_3)_2$
EDS	Energy dispersive x-ray spectroscopy
Ethanol	CH_3CH_2OH
Ethylene glycol	$HO–CH_2CH_2–OH$
FE-SEM	Field emission scanning electron microscope
Feldspar	$(K,Na,Ca)(AlSi)_4O_8$
Garnet	$(Mg,Fe,Mn,Ca)_3(Al,Fe_{3+})_2(SiO_4)_3$
Glutaraldehyde	$C_5H_8O_2$
Glutaric acid	$C_3H_6(COOH)_2$
Guar gum	$C_{12}H_{24}O_{12}$
Gypsum	$CaSO_4•2H_2O$
Halite	NaCl
Illite	$(K_{1.5\text{-}1.0}Al_4(Si_{6.5\text{-}7}Al_{1.5\text{-}1.0}O_{20})(OH)_4)$
Isopropanol	C_3H_8O
Kaolinite	$Al_2Si_2O_5(OH)_4$
Kieserite	$MgSO_4•H_2O$
Magnesite	$MgCO_3$
Methane	CH_4

Acronyms, Abbreviations, Symbols (cont.)

Term	Description
MNA	Monitored natural attenuation
Polyacrylamide	$CH_2CHCONH_2$
PolyDADMAC	Poly(diallyldimethylammonium chloride), $(C_8H_{16}NCl)_n$
Pyrite	FeS_2
Quartz	SiO_2
Rutile	TiO_2
SEM	Scanning electron microscope or scanning electron microscopy
Siderite	$FeCO_3$
Smectite	$(Ca,Na)_{.2\text{-}.4}(Al,Mg,Fe)_2(Si,Al)_4O_{10}(OH)_2{\cdot}nH_2O$
Strontianite	$SrCO_3$
Tourmaline	$(Na,Ca)(Mg,Fe,Mn,Li,Al)_3(Al,Mg,Fe^{3+})_6[Si_6O_{18}](BO_3)_3(O,OH)_3(OH,F)$
Zircon	$ZrSiO_4$

Acknowledgments

This work was completed as part of National Energy Technology Laboratory (NETL) research for the U.S. Department of Energy's (DOE) Complementary Research Program under Section 999 of the Energy Policy Act of 2005. The authors wish to acknowledge Ray Boswell (NETL Strategic Center for Natural Gas and Oil) and Elena Melchert (DOE Office of Fossil Energy) for programmatic guidance, direction, and support.

The authors would like to thank Keith Collins for helping debug the in-house SEM, and to everyone on Daniel Soeder's research team for their involvement with this research, including Daniel Soeder and Hank Edenborn for their reviews.

This page intentionally left blank.

EXECUTIVE SUMMARY

The Marcellus shale, located in the mid-Atlantic Appalachian Basin, has been identified as a source for natural gas and targeted for hydraulic fracturing recovery methods. Hydraulic fracturing is a technique used by the oil and gas industry to access petroleum reserves in geologic formations that cannot be accessed with conventional drilling techniques (Capo et al., 2014). This unconventional technique fractures rock formations that have low permeability by pumping pressurized hydraulic fracturing fluids into the subsurface. Although the major components of hydraulic fracturing fluid are water and sand, chemicals, such as recalcitrant biocides and polyacrylamide, are also used (Frac Focus, 2015).

There is domestic concern that the chemicals could reach groundwater or surface water during transport, storage, or the fracturing process (Chapman et al., 2012). In the event of a surface spill, understanding the natural attenuation of the chemicals in hydraulic fracturing fluid, as well as the physical and chemical properties of the aquifers surrounding the spill site, will help mitigate potential dangers to drinking water. However, reports on the degradation pathways of these chemicals are limited in existing literature.

The Appalachian Basin Marcellus shale and its surrounding sandstones host diverse mineralogical suites. During the hydraulic fracturing process, the hydraulic fracturing fluids come into contact with variable mineral compositions. The reactions between the fracturing fluid chemicals and the minerals are very diverse. This report: 1) describes common minerals (e.g. quartz, clay, pyrite, and carbonates) present in the Marcellus shale, as well as the Oriskany and Berea sandstones, which are located stratigraphically below and above the Marcellus shale; 2) summarizes the existing literature of the degradation pathways for common hydraulic fracturing fluid chemicals [polyacrylamide, ethylene glycol, poly(diallyldimethylammonium chloride), glutaraldehyde, guar gum, and isopropanol]; 3) reviews the known research about the interactions between several hydraulic fracturing chemicals [e.g. polyacrylamide, ethylene glycol, poly(diallyldimethylammonium chloride), and glutaraldehyde] with the minerals (quartz, clay, pyrite, and carbonates) common to the lithologies of the Marcellus shale and its surrounding sandstones;[1] and 4) characterizes the Berea sandstone and analyzes the physical and chemical effects of flowing guar gum through a Berea sandstone core.

[1] The existing literature for some mineral-hydraulic fracturing fluid pairs was limited.

1. INTRODUCTION

1.1 MINERAL CHARACTERIZATION

The Earth consists of thousands of minerals, but only a few constitute the majority of its crust. This section discusses commonly found minerals in the Berea and Oriskany sandstones and Marcellus shale. Understanding the mineralogy of a formation is important for recognizing how minerals influence natural processes and the impact that hydraulic fracturing may have on formations. Having a fundamental understanding of minerals and their potential reactions with their surroundings is paramount to understanding fracturing fluids' natural attenuation processes and the physical, chemical, and biological processes that reduce the concentration of fracturing fluids in a natural, subsurface environment (U.S. Geological Survey, 2015). The specific characterizations of the formations are discussed in greater detail in Section 2.

1.1.1 Quartz

Quartz (SiO_2) is the second most abundant mineral in the Earth's crust and is found in a wide range of igneous, metamorphic, sedimentary, and hydrothermal settings (Nesse, 2012). The hardness and lack of cleavage of quartz make the mineral resistant to additional weathering (Deer et al., 1992). Both the Berea and Oriskany sandstones are primarily composed of quartz.

1.1.2 Clays

Clay is composed of several different phyllosilicate minerals, which are also known as sheet silicates. Four of the more common types are kaolinite, chlorite, illite, and smectite. The atomic layering of some phyllosilicates electrostatically attracts liquid H_2O, allowing some phyllosilicates (smectite and illite, but not kaolinite or chlorite) to adsorb higher volumes of water than other mineral classes, promoting flocculation. Because of their structure, phyllosilicates contain variable amounts of alkali metals, alkaline earths, iron, and magnesium (Dana, 2008).

Chlorite [$(Mg,Fe^{2+},Mn,Al)_{12}((Si,Al)_8O_{20})(OH)_{16}$], is a common clay phyllosilicate, which forms primarily in low- to moderate-grade metamorphic rocks. Chlorite is heavily associated with slate, a common secondary lithology of the Marcellus shale. As the metamorphic grade of a rock increases, the rock's chlorite content decreases. Chlorite does not express exceptional water adsorption tendencies (Dana, 2008).

Kaolinite [$Al_2Si_2O_5(OH)_4$] is another common phyllosilicate clay mineral that forms where its parent materials, Al-rich minerals such as feldspar and muscovite mica, were deposited under non-alkaline conditions, like that of the Appalachian Basin. Kaolinite is also formed at shallow depths and low temperatures in mud rocks, clastic sediments, and coal (Deer et al., 1992). Kaolinite does not express exceptional water adsorption tendencies (Dana, 2008).

Illite [$K_{1.5\text{-}1.0}Al_4(Si_{6.5\text{-}7}Al_{1.5\text{-}1.0}O_{20})(OH)_4$], another common clay of the Appalachian Basin, is frequently produced by burial metamorphism from Al-rich minerals, including kaolinite and smectite (Deer et al., 1992). Illite expresses high water adsorption tendencies (Dana, 2008).

Although a common clay mineral worldwide, smectite is precluded from being a common mineral in the Appalachian Basin due to the area's thermal maturity (Deer et al., 1992; Rowan, 2006). The most common mineral in the smectite sub-group is montmorillonite [$(Ca,Na)_{0.3}(Al,Mg)_2Si_4O_{10}\cdot nH_2O$]. Much like kaolinite, montmorillonite is derived from Al-rich

minerals. Unlike kaolinite, montmorillonite varies in water content (Deer et al., 1992; Perkins, 2011). Smectite expresses high water adsorption tendencies (Dana, 2008).

1.1.3 Pyrite

Pyrite (FeS_2), an iron sulfide, is the most common sulfide mineral and is a reagent for the production of sulfuric acid (H_2SO_4), which is a common source of high stream acidity in regions where mining is prevalent, such as the Appalachian Basin. Oxygenated water interacts with pyrite to oxidize the iron, producing sulfuric acid as expressed in the following equation (Nesse, 2012):

$$2FeS_{2(s)} + 7O_2 + 2H_2O \rightarrow 2Fe^{2+}{}_{(aq)} + 4SO_2{}^{-4}{}_{(aq)} + 4H^+ \quad (1)$$

Pyrite is a common mineral in igneous, hydrothermal, and metamorphic rocks. Euxinic conditions, a common depositional environment of black shale, are also conducive for sulfide deposition (Deer et al., 1992). In shale and coal, pyrite is often present as fine-grained crystals or tiny, raspberry-shaped clusters called framboids. Pyrite is also produced by sulfate-reducing bacteria, converting Fe^{3+} into Fe^{2+}. In addition, pyrite may contain trace Ni^{2+} or Co^{2+} owing to metal substitution (Nesse, 2012). Some hydraulic fracturing fluids contain chemical compounds which could interact with pyrite through hydrolysis (Edwards et al., 2014).

1.1.4 Carbonates

Carbonates are formed by CO_3^{2-} bonding with a cation. The more commonly occurring carbonate cations are Ca^{2+}, Mg^{2+}, Mn^{2+}, Fe^{2+}, Fe^{3+}, Zn^{2+}, Ba^{2+}, Sr^{2+}, and Pb^{2+} (Nesse, 2012). Oil shale classification is based on carbonate composition (Yen and Chilingarian, 1976). Carbonate minerals tell of their depositional history and are discussed below.

Calcium carbonate ($CaCO_3$) is the most commonly occurring carbonate and naturally crystallizes as several polymorphs—calcite, aragonite, and vaterite. Calcite forms between clastic sediments as cement and in other environments as a biomineral, an evaporite, a hydrothermal deposit, and a metamorphic product. Aragonite and vaterite share the same chemical composition as calcite but express different crystal atomic lattice structures and stoichiometry due to their higher pressures of crystallization and the presence of trace enrichments (e.g. Ba, Mg^{2+}, SO_4^{2-}, Sr) (Berner, 1975; Walter, 1986; Nesse, 2012). Being the most common composition of carbonate minerals, calcium carbonates are prolific in the Appalachian Mountains.

Magnesite ($MgCO_3$) is common in Mg-rich metamorphic rocks, but is also frequently found mixed with $CaCO_3$ minerals in evaporite deposits and as a hydrothermal mineral. Unlike $CaCO_3$ minerals, magnesite is not a common biomineral but is common to the Appalachian Mountains (Nesse, 2012).

Dolomite [$CaMg(CO_3)_2$] is another common carbonate in the Appalachian Basin. Dolomite can be considered as the interlayering of calcite and magnesite at a 1:1 ratio. Fe^{2+} often replaces small amounts of Mg^{2+}. Dolomite is primarily a sedimentary rock, but metamorphic and hydrothermal occurrences are not uncommon (Deer et al., 1992). Several Appalachian limestones and marbles are composed predominantly of calcite and dolomite (Nesse, 2012). Deer et al. (1992) suggests that some dolomites are the product of Mg^{2+} released during the

breakdown of smectite to illite. Dolomite precipitation is favored in solutions with low Ca^{2+}/Mg^{2+} and Ca^{2+}/CO_3^{2-} ratios and high temperatures (Deer et al., 1992).

Siderite ($FeCO_3$) is a frequent trace carbonate in metamorphic rocks of sedimentary protoliths. Although Zielinski and McIver (1982) report the Marcellus shale to contain ~0% siderite, specific localities and members of the Marcellus have higher siderite concentrations; Soeder (2014) observed abundant siderite concretions up to tenths of a centimeter in size in the Oatka Creek Member of the Marcellus shale. Siderite is rarely found in pure form and, instead, contains low concentrations of Mn^{2+} and Mg^{2+} (Deer et al., 1992).

1.2 CHARACTERIZATION OF THE ORISKANY SANDSTONE, THE BEREA SANDSTONE, AND THE MARCELLUS SHALE

The Oriskany and Berea sandstone formations are located below and above the Appalachian Basin Devonian shales, which include the Marcellus shale (Figure 1), and are important stratigraphic units to understand in the context of hydraulic fracturing because of their proximity to the Marcellus shale. The Oriskany and Berea sandstones could be exposed to hydraulic fracturing fluids or provide means for hydraulic fracturing fluids to reach aquifers. Surface spills also pose a contamination hazard. Understanding the natural attenuation of the chemicals in hydraulic fracturing fluid and the physical and chemical properties of the aquifers surrounding a site of interest would help mitigate potential danger to human populations and the natural environment.

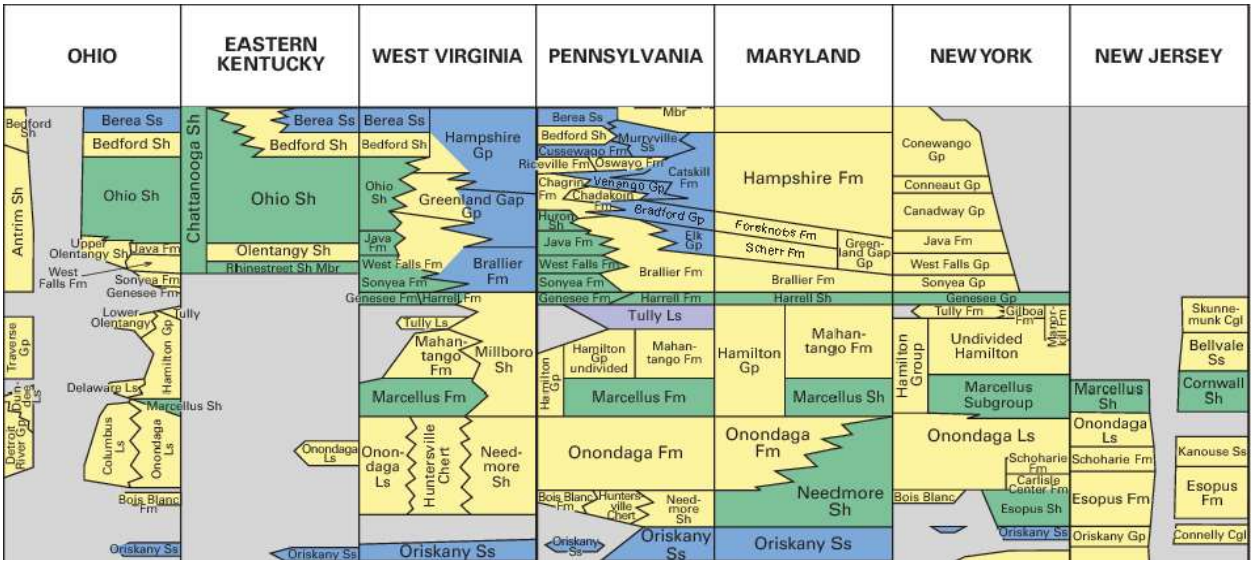

Figure 1: Stratigraphic column (modified from Midwest Regional Carbon Sequestration Partnership, 2015).

1.2.1 Oriskany Sandstone

The Oriskany sandstone (Figure 2) is a thoroughly studied geologic formation because of its proximity to the Marcellus shale and its use as a source for sand glass (Heinrich, 1981). The Oriskany sandstone interbeds with limestone, chert, and shale lithologies. Limestones are sedimentary rocks composed of calcium carbonate—specifically calcite and aragonite. Cherts are fine-grained sedimentary rocks that are silica rich but also incorporate surrounding minerals and elements into their structure. Shales are very fine mudstones composed mainly of clay minerals with some organic matter, iron, sulfide, and heavy mineral substitution. Common minerals found in these formations include quartz, calcium carbonates, kaolinite, illite, and chlorite (Dana, 2008).

Porosity throughout the Oriskany varies, averaging 4–7%, which is relatively low compared to the ~20% porosity of the majority of sandstones (Kostelnik and Carter, 2009). The Oriskany sandstone ranges from a fine- to medium- to coarse-grained sandstone with a cementing clay. The grains also tend to appear relatively weathered, rounded, and well sorted.

Figure 2: Oriskany sandstone outcrop in a U.S. Silica Quarry, Berkeley Springs, WV. Photo provided by Daniel Soeder and his research team with the National Energy Technology Laboratory, U.S. Department of Energy.

1.2.2 Berea Sandstone

The Berea sandstone (Figure 3) is also a thoroughly studied geologic formation because of its proximity to Appalachian Basin Devonian shales, its use as a test material for the petroleum industry, and its role as a resistant building material. Common minerals in the Berea sandstone are similar to the minerals found in the Oriskany, with quartz being the major mineral. Other minor components in the Berea sandstone include feldspar [$(K,Na,Ca)(Al,Si)_4O_8$] and chert, as well as heavy minerals, such as tourmaline[2], zircon ($ZrSiO_4$), rutile (TiO_2), chromite ($FeCr_2O_4$),

[2] $(Na,Ca)(Mg,Fe,Mn,Li,Al)_3(Al,Mg,Fe^{3+})_6[Si_6O_{18}](BO_3)_3(O,OH)_3(OH,F)$

apatite [$Ca_{10}(PO_4)_6(OH,F,Cl)_2$], garnet [$(Mg,Fe,Mn,Ca)_3(Al,Fe^{3+})_2(SiO_4)_3$], and barite ($BaSO_4$) (Pepper et al., 1954; Deer et al., 1992).

The Berea is fine-grained, clay-cemented quartz sandstone that is valuable for industrial purposes. While the chemical composition of the Berea sandstone is similar to the Oriskany sandstone, the Berea sandstone has higher porosity and permeability on average than the Oriskany sandstone. Average porosity and permeability values for the Berea are 21% and 165 mD (Jagucki and Darner, 2001). Groundwater in the Berea has a residence of ~2,500 years, an average pH of 7–8, and a dissolved oxygen concentration of 0–2 mg/L (Jagucki and Darner, 2001). In the field, the Berea seems coarser grained than it actually is because aggregates of fine grains are cemented together and appear as coarse grains. Field descriptions of the Berea vary from a medium-grained sandstone to a fine-grained pebbly sandstone to a coarse-grained pebbly siltstone with a cementing clay. The Berea sandstone encloses lenses of coarse pebble-like lithics composed of red shale, gray shale, black shale, and fine-grained steel-grey siltstone (Pepper et al., 1954).

Figure 3: Berea sandstone core from Cleveland Quarries, Vermillion, Ohio. The Berea core in this figure appears similar to the Berea core analyzed in this study. Photo provided by Daniel Soeder and research team with the National Energy Technology Laboratory, U.S. Department of Energy.

1.2.3 Marcellus Formation

The Marcellus Formation is a Devonian black shale in the Lower Hamilton group composed of organic, terrigenous sediments that accumulated in a trough that was formed from the impingement of Laurentia during the Acadian Orogeny that would later become the Appalachian Basin (Woodrow, 1985; Blauch et al., 2009; Enomoto et al., 2011). The Marcellus shale formed during sea-level fluctuations between shallowing and deepening conditions, sometimes under euxinic, H_2S-rich conditions (Sageman et al., 2003). Changes in sea level and climate resulted in saline evaporates interbedding with organic terrigenous sediments (Werne et al., 2002; Enomoto et al., 2011).

Shale is naturally heterogeneous. The Marcellus shale is no exception and hosts distinct lithofacies. One of the most important of the lithofacies is the argillaceous facies, which is dominated by quartz and clay minerals with minor amounts of halite (NaCl), calcite, mica, and pyrite. Boyce and Carr (2009) report high quartz contents (60%), relatively low illite-muscovite clay contents (30%), and pyrite contents between 5–10%. The other important lithofacies, the calcareous-argillaceous facies, are rich with calcite and contain only minor amounts of quartz. The trace minerals are barite, strontiantite ($SrCO_3$), celestite ($SrSO_4$), siderite ($FeCO_3$), gypsum ($CaSO_4 \cdot 2H_2O$), anhydrite ($CaSO_4$), and kieserite ($MgSO_4 \cdot H_2O$). The Marcellus also contains other minor lithofacies like the Purcell limestone, which is a fine grained, thin-bedded layer found within the Marcellus (Boyce and Carr, 2009). Other mineral features of the Marcellus include a saturation of halite and dolomitization from the saline evaporite formation (Bruner and Smosna, 2011).

The fluids involved with shale formation have an important effect on the mineralization during diagenesis. As Marcellus sediments were deposited and lithified, salts and fluids from the surrounding brine became incorporated into the rock structure. Once these pore fluids were mobilized, salt dissolution resulted in subsequent autochthonous crystallization within the rock's pore space (Blauch et al., 2009). Dresel and Rose (2010) found that oil field brines from the Devonian shales in Pennsylvania varied in concentration from 9.99 to 343 g/L total dissolved solids.

Organic-rich sediments heated in the Earth's crust produce kerogen, an insoluble organic mixture. Heating kerogen creates hydrocarbon chains, which vary in length and complexity depending on the temperatures to which the kerogen is exposed. Less heat equates to longer, more complex hydrocarbon chains (oil), but as heating increases, the chains become progressively shorter and simpler, producing wet gas and dry gas (Selley, 1997; McCarthy et al., 2011). The thermal maturity of the Marcellus shale makes wet and dry common hydrocarbon deposits (Repetski et al., 2008; Bruner and Smosna, 2011). Total organic carbon varies within the Marcellus Formation. Average values range from 2–5%, but can be as high as 12–20% (Nyahay et al., 2007; Laughrey et al., 2011; Wang and Carr, 2013). Ziemkiewicz et al. (2013) reported dissolved oxygen concentrations in Marcellus Formation groundwater between 3.24–13.12 mg/L and pH values of 6.32–8.75. As with the Berea and Oriskany sandstones, porosity also varies throughout the Marcellus. However, the porosity of shales is significantly lower than that of most sandstones. Laughrey et al. (2011) reported porosity between 2.44–16.6% of bulk volume and 2–4% organic porosity. They measured permeability of 0.047 to 0. 217 μD. Comparatively, Soeder (1988) found Marcellus porosity of 9.28% and of 19.613 μD. Estimates of porosity by the U.S. Department of Environmental Conservation (Leff, 2011) for Devonian shales in the Appalachian Basin are a tighter range of 1–3%.

1.3 HYDRAULIC FRACTURING FLUID CHEMICAL SUMMARY

Organic compounds in hydraulic fracturing fluids will degrade naturally through both microbiological and geochemical processes in groundwater, a process referred to as natural attenuation. Natural attenuation is utilized as a common remediation technique for groundwater contamination, and is referred to as monitored natural attenuation (MNA). For MNA to be effective, the breakdown processes and rates for the various chemicals must be understood. If MNA is shown to be too slow to prevent the contaminant from reaching the accessible environment, cleanup can be accelerated by the use of enhanced biodegradation, reactive

barriers, pump-and-treat, or other processes. This section reviews existing research for the natural attenuation of common hydraulic fracturing fluids.

1.3.1 Guar Gum

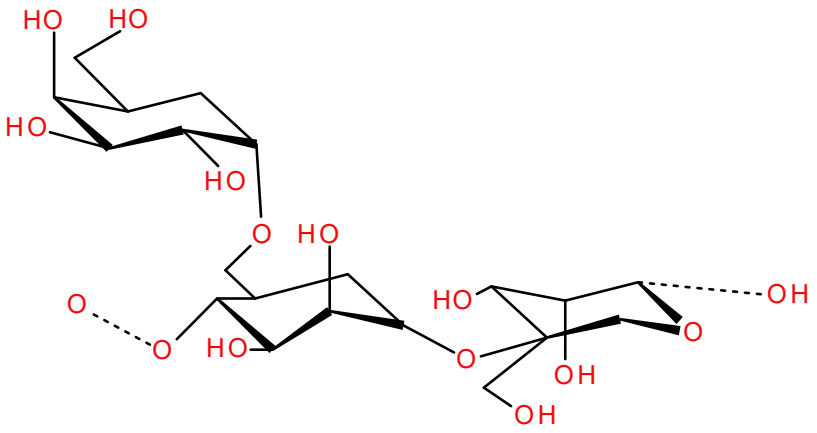

Figure 4: Skeletal chemical structure of guar gum. This figure depicts guar gum in skeletal formula format to communicate the complex molecule as a simple depiction. In a skeletal formula, carbon atoms are expressed as the end of line segments, and carbon-hydrogen bonds are assumed to bring carbon's valence to four.

Guar gum ($C_{12}H_{24}O_{12}$) (Figure 4) is a thickening agent used for carrying proppants into hydraulic fractures. A proppant is a solid material (usually sand) in hydraulic fracturing fluid used to prop open the fractures created by hydraulic pressure, maintaining open flow paths after the pressure has been released (Frac Focus, 2015). Most of the previous research related to guar gum focuses on guar gum breakdown in the digestive tract, because guar gum is used as a thickening agent in many food products such as ice cream. It has not been thoroughly studied because it is non-toxic to humans, but it still has the potential to chemically and physically interact with microbes and other chemicals. Insoluble residues like protein and cellulose are associated with guar gum and can reduce the flow of gas out of the well after the guar gum degrades. Solutions below pH 5 and above pH 7 can cause hydrolysis of guar gum. Fermentation of guar gum produces short-chain fatty acids and gases such as carbon dioxide, hydrogen, and methane (Mali et al., 2012).

Salyers et al. (1977 and 1978) studied the degradation of guar gum by anaerobic microorganisms. They found that *Bacteroides ovatus*, *Bacteroides '0061-1,'* and *Bacteroides vulgatus* ferment guar gum. Additionally, they found that the enzymes responsible for the degradation of the guar gum were extracellular and inducible. Extracellular enzymes are attached on the outside of the cell but are still part of the organism. Complex and bulky substrates are able to react with extracellular enzymes without having to move into the interior of the cell. Inducible enzymes are adaptable and can be turned on or produced when the substrate is present. The end products of fermentation will depend on the microorganism that is biodegrading the guar gum, but the most common end products are acetate, butyrate, propionate, and lactate. Hartemink et al. (1999) discovered that *B. ovatus* produces mainly acetate and propionate; *Ruminococcus albus* produces acetate and a small amount of butyrate; *Bifidobacterium adolescentis* produces acetate

and lactate; *Clostridium butyricum* produces butyrate; *Clostridium coccoides* produces succinate; and *Ruminococcus productus* produces acetate.

1.3.2 Polyacrylamide

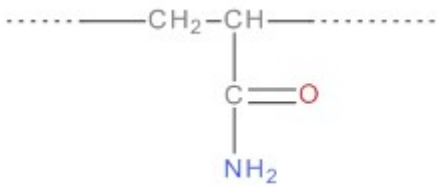

Figure 5: General chemical structure of polyacrylamide.

Polyacrylamide (–$CH_2CHCONH_2$–) (Figure 5) is a synthetic, industrial polymer that decreases the friction of the hydraulic fracturing fluids and is sometimes referred to as "slickwater" (Frac Focus, 2015). While polyacrylamide itself is non-toxic, acrylamide monomers created during breakdown are toxic to peripheral nerves. This is not unusual in the degradation process; many organic chemicals produce daughter products or "metabolites" that are more toxic than the original compound. A complete understanding of the breakdown path from start to finish is required to assess if MNA is a viable remediation option for any particular compound.

Acrylamide monomers are produced from abiotic degradation of polyacrylamide by heat or ultraviolet irradiation, so the degradation of polyacrylamide is an important chemical pathway to study. Wen et al. (2010) isolated polyacrylamide-metabolizing bacteria, *Bacillus cereus* and *Bacillus flexu*, and identified polyacrylamide as their sole source of carbon. The addition of glucose to the substrate at low concentration (below 200 mg/L) increased the rate of biodegradation and can be co-metabolized with polyacrylamide. Conventional carbon sources (i.e. glucose) at lower concentrations stimulate growth which leads to more enzymes to breakdown toxic compounds; however the microbes will prefer to metabolize the additional organic carbon over the toxic compounds which leads to a decrease in biodegradation (Wen, et al., 2010). The highest rate of biodegradation that Wen et al. (2010) observed was roughly 70% over 96 hours of cultivation at low initial concentrations of polyacrylamide. However, with an initial concentration of 500 mg/L, *B. cereus* degrades roughly 50% over 96 hours, and *B. flexu* only degrades roughly 30% over 96 hours.

In addition to Wen et al. (2010), other studies have focused on other organisms' effects on the degradation of polyacrylamide. Stahl et al. (2000) studied the white-rot fungi, *Phanerochaete chrysosporium*, which degrades lignin along with a variety of environmental toxins, including polyacrylamide. The enzymes responsible for extracellular degradation catalyze polyacrylamide in manganese and iron redox reactions. Adding sawdust and soil microbes to the white-rot fungus optimized biodegradation conditions. Solubilization of the polyacrylamide was the rate-limiting step in this biodegradation experiment (Stahl et al., 2000). Nakamiya and Kinoshita (1995) isolated bacteria (*Enterobacter agglomerans* and *Azomonas macrocytogenes*) that metabolized polyacrylamide using a substrate of 10 mg/mL of polyacrylamide as their sole carbon and nitrogen source. *E. agglomerans* is an anaerobic bacterium, while *A. macrocytogenes* is an aerobic bacterium. Both bacteria only degraded a proportion of initial polyacrylamide at

10 g/L (utilized to available polyacrylamide). However, when comparing real commercial polyacrylamide to the lab-synthesized polyacrylamide, the growth of the bacteria was delayed, and the degradation ratio was almost half of the rates seen with the lab polyacrylamide.

Kay-Shoemake et al. (1998) found microbes utilizing polyacrylamides as a nitrogen source. Wang and Lee (2001) isolated denitrifying bacteria, *Pseudomonas stutzeri*, that use acrylamide as a substrate for metabolism and observed the degradation of acrylamide under aerobic and anaerobic conditions. *P. stutzeri* produced ammonia and acrylic acid as intermediates. Under aerobic conditions, *P. stutzeri* metabolized acrylamide at different efficiencies, depending on the concentration. Initial concentrations up to 148.9 mg/L of acrylamide were 91% removed after 5.9 hours and 100% removed after 10 hours. Initial concentrations up to 440.1 mg/L of acrylamide were 53% removed after 6 hours and 80% removed after 14.1 hours. Ammonia and acrylic acid were intermediate products of acrylamide biodegradation and act as carbon and nitrogen sources under aerobic conditions. Under anaerobic conditions, *P. stutzeri* metabolized 100% of 148.9 mg/L acrylamide with 147.3 mg/L nitrate after 15.8 hours. Wang and Lee (2001) found that, "With the existence of adequate electron acceptors, the *P. stutzeri* could utilize both acrylamide and acrylic acid as the substrates undergoing denitrification, and acrylamide could be removed completely from the wastewater."

1.3.3 Ethylene Glycol

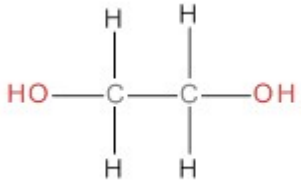

Figure 6: Chemical structure of ethylene glycol.

Ethylene glycol ($HO–CH_2CH_2–OH$) (Figure 6) compounds are used in addition to pH stabilizers to inhibit CO_2 corrosion of the drilling infrastructure (Frac Focus, 2015). Ethylene glycol prevents the formation of hydrates, which can form when the pH stabilizers increase the pH of the solution to inhibit corrosion. The anaerobic degradation of ethylene glycol, using nitrate as an electron acceptor, produces methane and carbon dioxide as end products. Intermediate products include acetaldehyde, ethanol, acetate, and bicarbonate (Dwyer, 1986 Schramm and Schink, 1991; Huang et al., 2005). The degradation pathway of ethylene glycol under anaerobic methanogenic conditions is shown in Table 1 (Veltman et al., 1998).

Gruden et al. (2001) observed glycolic acid and oxalic acid as intermediate products and carbon dioxide as the final end product of anaerobic degradation of ethylene glycol. Dwyer et al. (1986) isolated two anaerobic bacteria from methanogenic cultures that metabolized polyethylene glycols. One of the bacteria, *Desulfovibrio desulfuricans*, explicitly metabolized ethylene glycol. The other bacteria, *Bacteroides* (strain PG1) metabolized diethylene glycol and polymers of polyethylene glycol but could not metabolize ethylene glycol. Both bacteria used polyethylene glycol as the sole carbon source, and both grew well in coculture with sulfate and methanogenic

bacteria acting as an electron acceptor producing acetate, ethanol, and hydrogen as end products with acetaldehyde as an intermediate product. The substrates that did not support growth of the bacteria and fermentation of polyethylene glycols were glycolate, glyoxylate, glycerol, ethanolamine, polyoxyethylene sorbitan monolaurate, polyoxyethylene 23-lauryl ether, and polypropylene glycols. Additionally, de Ory et al. (1998) found that the bacteria, *Acetobacter aceti*, metabolizes ethanol to acetate, and after all of the ethanol is converted, they metabolize the available CO_2.

Table 1: Anaerobic decomposition of ethylene glycol (Veltman et al., 1998)

Reaction	Chemical Equation	ΔG (Kcal)
Ethylene Glycol → Acetate + Ethanol	$HOCH_2CH_2OH \rightarrow 0.5\ CH_3COO^- + 0.5\ HC + 0.5\ CH_3CH_2OH + 0.5\ H_2O$	-21.7
Ethanol → Acetate	$CH_3CH_2OH + H_2O \rightarrow CH_3COO^- + HC + 2\ H_2$	2.3
Ethylene Glycol → Acetate	$HOCH_2CH_2OH \rightarrow CH_3COO^- + HC + H_2$	-20.6
Acetate → Methane	$CH_3COO^- + H_2O \rightarrow HCO_3^- + CH_4$	-7.4
Hydrogen → Methane	$4\ H_2 + HC + HCO_3^- \rightarrow CH_4 + 3H_2O$	-32.4
Ethylene Glycol → Methane	$HOCH_2CH_2OH + 0.25\ H_2O \rightarrow 1.25\ CH_4 + 0.75\ HC + 0.75HCO_3$-	-36.1

1.3.4 Poly(Diallyldimethylammonium Chloride)

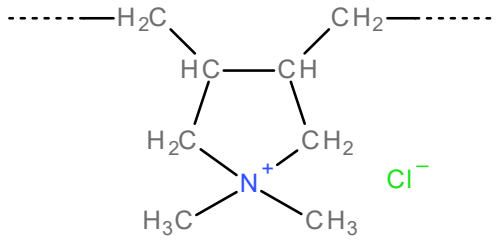

Figure 7: Chemical structure of poly(diallyldimethylammonium chloride).

Poly(diallyldimethylammonium chloride) (polyDADMAC) $(C_8H_{16}NCl)_n$ (Figure 7) is a polymer used for flocculation in hydraulic fracturing processes (Morrison and Boyd, 1987). PolyDADMAC falls within the larger chemical category of quaternary ammonium compounds. Morrison and Boyd (1987) studied quaternary ammonium compounds' reactions to different pH conditions and found quaternary ammonium compounds to be largely unaffected by pH changes as ammonium compounds have no protons to give and are unaffected by OH^-. However, at high pH extremes, a quaternary ion may form a hydroxide that can undergo a Hoffman elimination reaction.

John (2008) used a novel approach—gel permeation chromatography—to study polyDADMAC's reactivity under varied temperature, pH, and microorganism conditions. PolyDADMAC appears to be a stable polymer resistant to a range of varying environmental conditions. John (2008) subjected polyDADMAC to a range of temperatures from ambient to 80°C. Between ambient temperatures and 70°C, no structural changes to the polymer were observed. Between 70°C and 80°C, gel permeation chromatography displayed evidence of scission between the long and short chains, but new product formation was not evident. However, in the same study, John (2008) adjusted the polyDADMAC solution (0.5% m/v) pH by adding phosphoric acid (10% v/v) and sodium hydroxide (0.1 N). The pH conditions were held for 1 hour. Analysis revealed polyDADMAC to be resistant to pH conditions ranging 2–12. Acidic and moderately basic solutions displayed no evidence of new products. Highly basic solutions (> pH 12) displayed some evidence of new product, but concentrations were too low for identification.

John (2008) inoculated two aliquots of 0.02% polyDADMAC solution—one with 200 µL of *Candida albicaris* (yeast) and the other with a 25 mL aliquot with *Bacillus subtilis* (bacteria). These two solutions were incubated at 30°C for a minimum of 48 hours. Analyses from the *C. albicaris* and *B. subtilis* cultures indicated some biodegradation, but John (2008) does not specify a concentration or composition of the new product. John (2008) also attempted similar tests with *Escherichia coli* and coliforms, but was unsuccessful due to the death of the cultures.

1.3.5 Glutaraldehyde

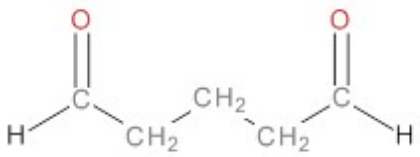

Figure 8: Chemical structure of glutaraldehyde.

Glutaraldehyde ($C_5H_8O_2$) (Figure 8) is the most common electrophilic biocide used during hydraulic fracturing and is frequently used as a disinfectant in the medical field (Kahrilas et al., 2015; Frac Focus, 2015). Although the literature regarding glutaraldehyde's interaction with minerals is virtually non-existent, glutaraldehyde's degradation processes are well studied. Glutaraldehyde functions by damaging cellular walls of the organisms to which it is exposed (Kahrilas et al., 2015).

Leung (2001a) summarizes numerous glutaraldehyde toxicity studies. The median effective concentration for glutaraldehyde (EC_{50}) was found to be 25 mg/L for sewage bacteria, 17 mg/L for Polyseed® (Polybac Corp.) bacteria, and 0.78 mg/L for oysters (Kahrilas et al., 2015). The No Observed Effect Concentration was found to be 5 mg/L, above which glutaraldehyde inhibited microbial behavior over prolonged exposure. Emmanuel et al. (2005) studied the toxic effects of glutaraldehyde when in solution with three commonly used hospital surfactants (cetyltrimethylammonium bromide, sodium dodecyl sulfonate, and Triton X-100) on *Vibrio fischeri* and *Daphnia*, but mixing did not increase impact. Glutaraldehyde appears resilient to abiotic degradation. A 50-mL, 2-mg/L sample of glutaraldehyde displayed no degradation in the

dark at 20°C after 28 days. However, 50°C produced ~8% degradation after 14 days (Leung, 2001a).

Glutaraldehyde is not strongly susceptible to hydrolysis in acidic or neutral pH environments, but it is unstable in alkaline environments. At 25°C, 50% degradation took 508 days in a pH 2 environment, 102 days in a pH 7 environment, and 46 days in a pH 9 environment. Leung (2001a) identified the degradation product as a cyclized dimer of glutaraldehyde (3-formyl-6-hydroxy-2-cyclohexene-1-propanal). Glutaraldehyde can be deactivated by two methods. In the first, concentrations up to 5% glutaraldehyde can be deactivated by adding 2–3 molar parts sodium bisulfate ($NaHSO_3$) to the solution. Deactivation is complete after 10 minutes. In the second method, NaOH, KOH, or dibasic ammonium phosphate is added to a pH 12 solution with glutaraldehyde. The glutaraldehyde becomes deactivated in ~8 hours and produces a cyclicized dimer (3-formyl-6-hydroxy-2-cyclohexene-1-propanal). As the acidity increases, deactivation time increases (Leung, 2001b).

1.3.6 Isopropanol

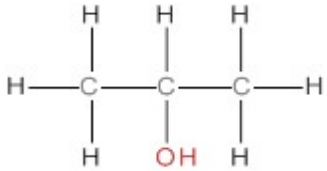

Figure 9: Chemical structure of isopropanol.

Isopropanol (C_3H_8O) (Figure 9) inhibits corrosion and increases viscosity of the fluid in hydraulic fracturing (Frac Focus, 2015). It is widely used for industrial purposes and can be oxidized to acetone, which can be metabolized by bacteria. Biodegradation has been observed under anaerobic conditions (Ueyama et al., 1971; Fox and Ketha, 1996), at low concentrations (Murrays et al., 1980; Kanemitu et al., 1980), and at high concentrations (Inoue and Horikoshi, 1989; Moriya and Horikoshi, 1993). Isopropanol can be toxic to some microorganisms but can be the main carbon source for denitrifying bacteria (Hwang et al., 1995). Quinlan et al. (1999) described the isopropanol-degrading bacteria's substrate preferences, specific growth rate, and solvent-tolerance. Siegel and Kamen (1950) studied the anaerobic microbe *Rhodopseudomonas gelatinosa* that metabolized isopropanol, acetone, n-butanol, n-hexanol, ethylmethyl ketone, acetic acid, propionic acid, butyric acid, and acetoacetic acid. Acetone was produced as an intermediate product of isopropanol degradation, accumulated, and metabolized by *R. gelatinosa*. The growth rate of *R. gelatinosa* increased with the addition of 0.3% Difco peptone and 200 mg/L of dehydrated yeast.

Bustard et al. (2001) studied the biodegradation of isopropanol by a consortium of bacteria in an aerobic three-phase fixed bed bioreactor. Bustard et al. (2001) claimed that a consortium of a mixed population of microorganisms is more successful at biodegradation than an isolated microorganism. The consortium was cultivated by enriching a sample from an oil waste sump with hydrocarbons and isopropanol. This allowed the isopropanol-biodegrading microorganisms to thrive. The consortium degraded 96% of the initial concentration of isopropanol (0.785 g/L)

after 80 hours of treatment. The rate of biodegradation fluctuated between 3.9 x 10^{-3} g/L/h and 300 x 10^{-3} g/L/h with an average degradation rate of 80 x 10^{-3} g/L/h. While Bustard et al. (2001) did not isolate and identify the specific bacteria in the consortium, they did observe that the degradation pathway is similar to the degradation mechanisms of *Xanothobacter* sp. and *Rhodococcus rhodachrous*.

1.4 MINERAL-HYDRAULIC FRACTURING FLUID CHEMICAL RESEARCH

Hydraulic fracturing fluids emplaced at depth are introduced to the mineralogies of the rock units targeted for hydraulic fracturing. Loss of hydraulic fracturing fluids at the surface can also lead to groundwater infiltration and affect shallow aquifers. Understanding the reactions and interaction between the hydraulic fracturing fluids and the mineralogy is key to the hydraulic fracturing fluids' natural attenuation in a subsurface environment. The literature surrounding these interactions does not cover every hydraulic fracturing fluid and commonly occurring mineral. This report summarizes the literature available that describes these interactions.

1.4.1 Polyacrylamide

Polyacrylamide—Quartz

Quartz-polyacrylamide research focuses on the adsorption of polyacrylamide onto the crystal's surface. However, whether non-ionic polyacrylamide adsorbs to quartz crystals has not yet been determined (Samoshina et al., 2003). Lecourtier et al. (1990) found evidence supporting non-ionic polyacrylamide adsorption to be temperature-based. Bjelopavlic et al. (2000) postulated that the surface charge of quartz depends on too many parameters to allow for consistent non-ionic polyacrylamide adsorption. Guevellou et al. (1995) reported more adsorption with anionic than non-ionic acrylamide. Samishona et al. (2003) found cationic polyacrylamide to adsorb well (.8-1.8 Γ mg/m^2) on quartz crystals, whereas anionic polyacrylamide adsorbed, but to a lesser extent (0.1–0.3 Γ mg/m^2). Guevellou et al. (1995) found aluminate—a compound containing oxygen, aluminum, and other metals—to precipitate out of a cationic polyacrylamide-sand-kaolinite-aluminate mixture after 5–10 days. Precipitation did not occur when an anionic polyacrylamide was used in place of the cationic polyacrylamide (Guevellou et al., 1995).

Polyacrylamide—Clay

Kaolinite adsorbs polyacrylamide by a factor of three more than quartz. Graveling et al. (1990) postulates that kaolinite's greater adsorption characteristic is a product of the mineral's basal planes. Tekin et al. (2005) suggested kaolinite adsorption of cationic polyacrylamide increases with pH, temperature, and ionic strength. The increased adsorption ability of kaolinite allows polyacrylamide to serve as an electrostatic stabilizer for kaolinite (Tekin et al., 2005). Polyacrylamide causes clays to increase in volume, strength, pore space, and permeability (Wallace and Wallace, 1986). When serving as a flocculent, cationic polyacrylamides create a larger floc size than anionic polyacrylamides. However, increasing the charge for cationic and anionic polyacrylamides by between 10–35% decreases the floc size (Nasser and James, 2007).

Polyacrylamide—Carbonates

Peng and Garnier (2012) demonstrated that the floc size of calcium carbonates increases as a function of the cationic polyacrylamide charge density. Smaller polyacrylamide chains express a higher charge density. When NaCl was added to the mixture, this relationship was reversed.

Wang et al. (2006) precipitated aragonite from a $Ca(OH)_2$ and CO_2/N_2 gas mixture in a polyacrylamide substrate as expressed in the following equation.

$$Ca(OH)_2 + CO_2 \rightarrow CaCO_3 + H_2O \quad (2)$$

Polyacrylamide—Pyrite

The literature on pyrite-polyacrylamide interaction is sparse, which is surprising given pyrite's common occurrence in coal extraction and other industrial processes. Boulton et al. (2001) developed a method using low-weight polyacrylamides to separate sphalerite (ZnS), a zinc ore, from pyrite.

1.4.2 Ethylene Glycol

Ethylene Glycol—Clay

Clays do not appear chemically active to ethylene glycol at surface temperatures and pressures. Hosterman and Whitlow (1983) found no evidence of chemical change in clays that were mixed with ethylene glycol and raised to a temperature of 350°C for 30 minutes. An XRD sample preparation manual advises to apply ethylene glycol on illite and smectite to induce swelling for a better analysis (Poppe et al., 2002). This practice suggests ethylene glycol and clays are not chemically active on a short-term timescale. Kaolinite and chlorite do not swell from ethylene glycol contact (Hosterman and Whitlow, 1983).

Ethylene Glycol—Carbonates

Ethylene glycol's role in preventing calcium carbonate buildup in industrial applications has helped foster ethylene glycol-carbonate research. Flaten (2009) studied the effect of ethylene concentration on calcium carbonate precipitation. Solutions with high ethylene glycol concentrations produced vaterite, while higher temperature solutions of the same composition produced aragonite. Flaten (2009) postulated that ethylene glycol extends the life of metastable polymorphs (e.g. vaterite) by delaying the growth of more stable polymorphs (e.g. calcite). Flaten et al. (2010) studied the relationship between the induction time of calcium carbonate precipitation and ethylene glycol. At 90 weight percent ethylene glycol and 25°C, $CaCO_3$ required an induction time of 12 days. Increasing the ethylene glycol content increased the required induction time. Maintaining constant ethylene glycol concentrations while lowering temperatures also increased the calcium carbonate induction time. Similarly, increasing the ethylene glycol concentration increased the nucleation rate but decreased the crystal growth rate (Konopacka-Konopacka-Łyskawa and Lackowski, 2011). These effects are likely due to CO_2's decreased solubility in ethylene glycol (Hayduk and Malik, 1971).

Ethylene Glycol—Pyrite

Ethylene glycol-pyrite reactions do not receive the same attention as ethylene glycol-calcium carbonate reactions. Mahajan et al. (2007) added ethylene glycol to hydrogen peroxide and chalcopyrite to stabilize the hydrogen peroxide without altering the chalcopyrite morphology. This resulted in increased Cu^{2+} dissolution and leaching efficiency. In another study, Wang et al. (2011) used ethylene glycol (after homogenized iron chloride hexahydrate and dimethyformamide solution) to assist with the precipitation of nanoflakes-built pyrite

microspheres and argued that this method could be used to precipitate other chalcogenides, such as PbS and Cu_xS.

1.4.3 Glutaraldehyde

Glutaraldehyde—Sediments

Leung (2001b) studied the biodegradation of glutaraldehyde when added to water and sediments from the Sacramento River. Under aerobic degradation, glutaraldehyde had a half-life of 10.6 hours and was completely metabolized after 48 hours. Glutaraldehyde degraded to an intermediate-stage glutaric acid before being completely metabolized to CO_2 (Figure 25). Under anaerobic degradation, glutaraldehyde had a half-life of 7.7 hours and completely metabolized after 72 hours. Glutaraldehyde degraded to an intermediate-stage 5-hydroxypentanal before being completely metabolized to 1,5-pentanediol (Figure 10).

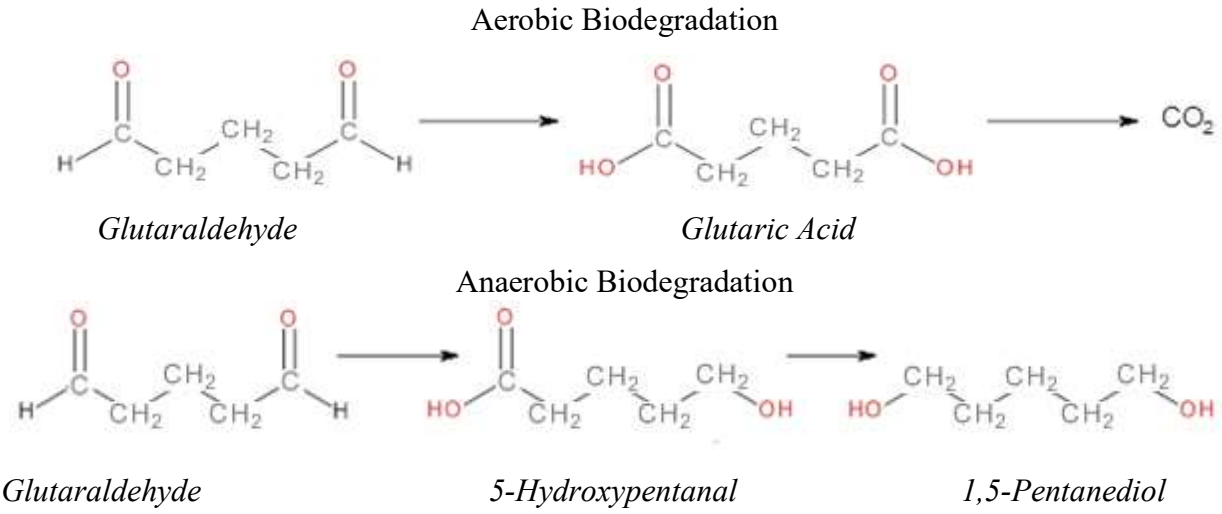

Figure 10: Aerobic and anaerobic biodegradation of glutaraldehyde.

Glutaraldehyde autopolymerizes via aldol condensation into *α,β*-unsaturated polymers that are not classified as toxic (Kahrilas et al., 2015). Landrum et al. (2003) observed that higher temperatures (5°C vs. 15°C vs. 25°C), higher concentrations of microorganisms, and lower concentrations of glutaraldehyde accelerated the rate of biotic glutaraldehyde degradation, but they found no difference in abiotic degradation rates between water-only and water-sediment samples. At and below 4°C, biotic degradation appeared to effectively cease. Landrum et al. (2003) found glutaraldehyde's abiotic degradation over 28 days to be inconsequential at temperatures below 25°C and did not run samples above 25°C.

1.4.4 Poly(diallyldimethylammonium chloride)

This literature review found no information involving specific quartz, clay, pyrite, or carbonate interaction.

1.4.5 Natural Attenuation Summary

The natural attenuation literature regarding hydraulic fracturing fluids suggest that understanding the mineral suites, bacterial presence, and physical conditions of a spill site are just as important as knowing which chemicals are present at the spill. The degradation pathways of hydraulic fracturing fluids are complex and highly dependent on the pH, redox state, mineral compositions, and bacterial species in the soil and shallow aquifers that may be affected by a spill. Additional research on specific degradation pathways involving different organic chemicals and fluid compositions would aid in increasing the understanding of potential environmental effects of hydraulic fracturing in the Appalachian Basin. This study of the interaction between guar gum and the Berea sandstone is one such attempt to observe how hydraulic fracturing fluid chemicals may interact with the lithologies of the Appalachian Basin.

2. METHODS

The experiment in this study isolates reactions caused by one additive in hydraulic fracturing fluid: guar gum. Guar gum was chosen for the initial natural attention study because it is extremely common in hydraulic fracturing operations and may be a strong contributor to microbial reactions. Guar gum is used as a gelling agent to suspend proppant transported to the fractures at depth. This organic chemical is used in food products and is easily degraded by biological processes.

The guar gum was mixed with tap water to a concentration of 3 mg/mL before introduction to the Berea core from Cleveland Quarries, Vermillion, Ohio as described in Section 1.2.2 (13 cm long, 5 cm in diameter). The Berea core, enveloped in a sleeve, was placed under confining pressure of 500 psi and connected to an Isco syringe-pump, which forced fluid through at a constant rate of 0.04 mL/min. The confining pressure on the sleeve forced the guar gum to flow through the core rather than around the outside. Effluent was collected at the downstream end. The experiment was performed until the pressure needed to force the guar gum through the Berea core reached 20 psi. This pressure likely increased due to guar gum filling pore spaces and preventing aqueous flow. Over the duration of the test, approximately 360 ml of water/guar gum solution passed through the Berea core. It took approximately 40 hours from the time that the guar gum was introduced to the system until it was observed on the downstream end of the Berea core. Samples were collected to measure the concentration of guar gum in the effluent and extrapolate the amount of guar gum retained in the core. After shutting down the experiment, the guar gum-exposed Berea core was allowed to sit for 36 days before being removed from its sleeve and core-holder apparatus and then cut into 3-cm thick pucks, using a diamond saw wetted with 0.25 ounces of Struers cooling fluid per 1.5 gallons of tap water. After cutting, the pucks were rinsed with de-ionized water. These samples were placed in zip-lock plastic bags and shipped for analysis. Upon arrival, initial samples were impregnated with an epoxy, polished down to a 3-µm diamond grit, and coated with palladium. However, the carbon-rich epoxy interfered with carbon detection limits during analysis. A second set of samples were prepared with no epoxy to avoid altering the guar gum microstructure.

To analyze the geochemical effects of guar gum on the Berea sandstone core, a field emission scanning electron microscope (FE-SEM) FEI Inspect F was used to examine the sandstone before and after interaction with guar gum. The inflow and outflow ends of the sample were compared. A SEM back-scattered electron (BSE) detector allowed identification of compositional boundaries, specifically cemented grains and organics. A sample's composition determines the degree to which electrons will be backscattered because BSE rates correlate with atomic number; heavier elements produce stronger backscattering, which appears brighter in images. In addition, energy dispersive X-ray spectroscopy (EDS) permitted elemental X-ray mapping, elemental distribution, and spot analysis of the sample. SEM has inherent limitations when characterizing sandstones, which are particularly susceptible to charging due to clay grains and Fe-rich inclusions. For analysis, an accelerating voltage ranging 12–18 keV was used with a spot size 4–5. Elemental intensities were determined by internal standards that were manually set into Oxford-INCA software interfaced with the SEM and optimized with copper. Porosity changes were completed qualitatively by comparing before and after images in area covered by guar gum.

3. OBSERVATIONS AND DISCUSSION

3.1 BEREA SANDSTONE ANALYSIS

The Berea sandstone is composed of ~95% angular quartz with trace amounts of clays, feldspar, and heavy minerals. The quartz grains express conchoidal fracturing and are dissolute along the sharp edges of the grains and the pore-grain interface. Most of the non-quartz minerals are clays (e.g. kaolinite and illite) and feldspars. Cementation and recrystallization appear along the edges of the Berea sandstone pores. The main components of Berea sandstone are oxygen, silica, alumina, and carbon (Figures 11). Trace amounts of other elements, such as potassium, calcium, iron, sulfur, chlorine, magnesium, and sodium, have also been discovered (Figure 11). Figure 12 shows that the pore spaces, which vary in size (< 20–100µm), have extensive connectivity and are mostly angular. The pores are continuous and close in proximity.

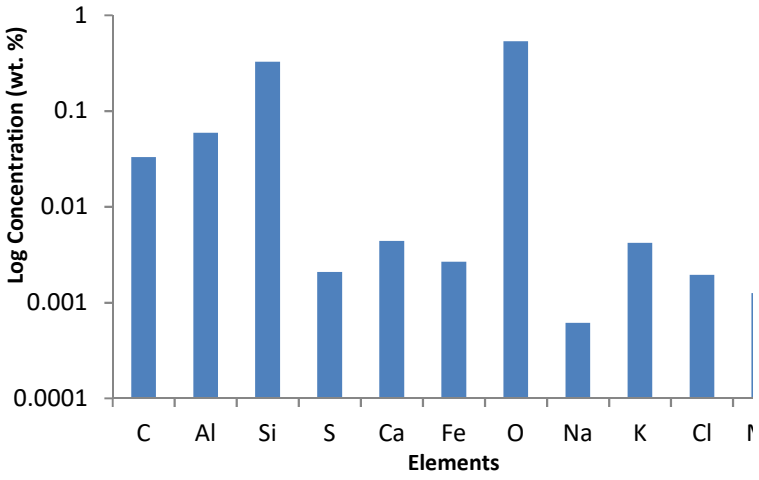

Figure 11: Composition of the Berea sandstone (log scale of the relative weight percent).

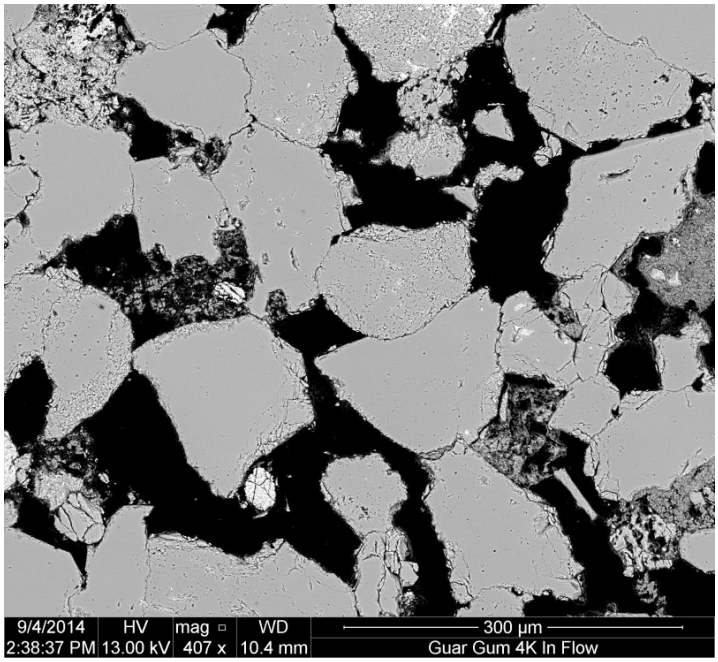

Figure 12: SEM-BSE image of the angular porosity of the Berea sandstone.

3.2 BEREA-GUAR GUM FLOW-THROUGH ANALYSIS

The remainder of this report focuses on the geochemical and microstructural changes of the Berea sandstone once guar gum has been injected. A general trend is that the guar gum is higher in concentration near the injection site and decreases rapidly (<6 cm) toward the outflow. As a result, guar gum covers a significant portion (>50%) of the inflow surface, whereas the guar gum is less prevalent (<1% surface coverage) on the outflow surface. Figure 13 contrasts the inflow and outflow surfaces of the Berea sandstone sample of this experiment. The Berea's pores on and near the inflow surface are blocked by the guar gum, which decreases the sandstone's effective porosity and permeability; however, the farther the distance away from the inflow surface, the more porosity and permeability return to unaltered levels. Figure 14 depicts the original porosity of pristine Berea sandstone compared to Berea sandstone post-flow-through. The higher concentration of guar gum on the inflow surface compared to on the outflow surface is likely a result of guar gum's partial insolubility and suggests that the guar gum may prevent further flow due to plugging of the pores, which inconsistent with guar gum rheological studies (Weaver et al., 2003; Kawamura, 2008; Gastone et al., 2014).

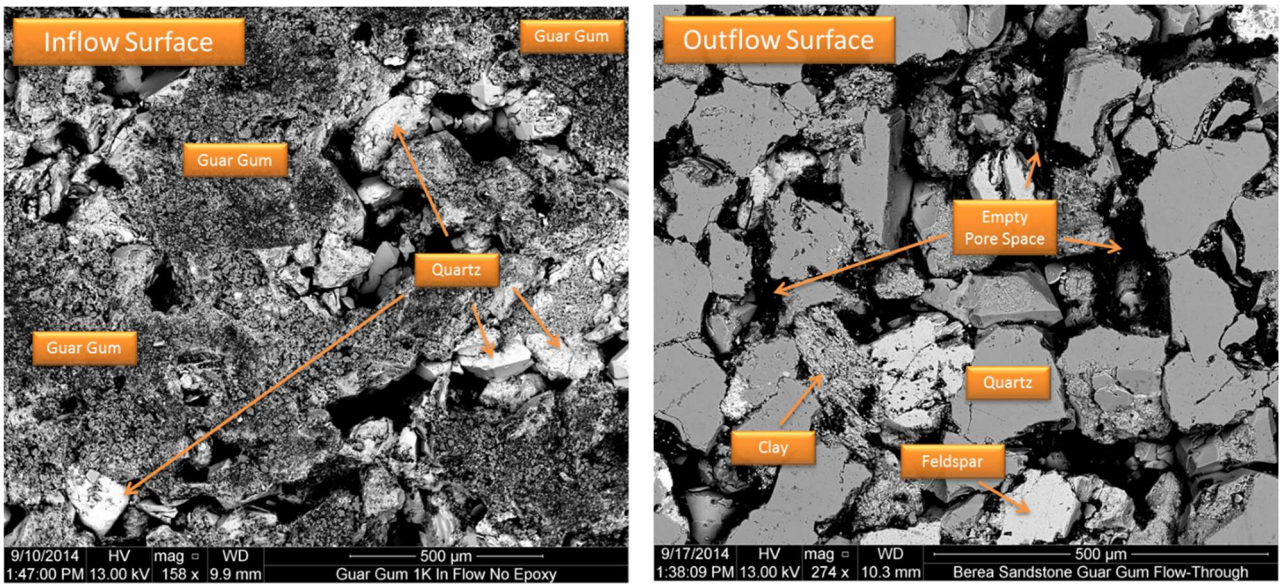

Figure 13: SEM-BSE images of post-guar gum inflow and outflow surfaces.

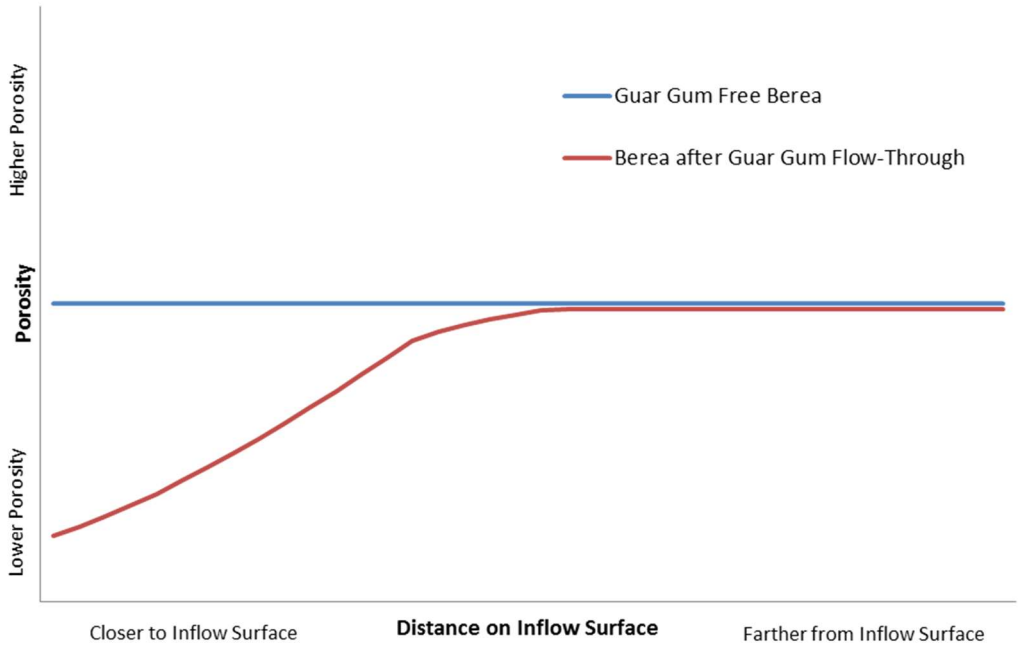

Figure 14: Porosity changes after guar gum flow-through experiment. Unaltered Berea sandstone has similar porosity throughout its entirety (blue). The modal abundance of guar gum is higher closer to the inflow surface resulting in lower porosity; as the abundance decreases, the effective porosity increases across the core (red).

3.2.1 Inflow Surface: Berea-Guar Gum Flow-Through Analysis

SEM-BSE images (Figures 15, 16, 17) show that the guar gum is not uniformly distributed across the post-flow Berea sample, but it appears to stay in contiguous volumes. The quartz within the Berea sandstone itself did not appear to change chemically; however, the injection of the viscous guar gum into the Berea sandstone resulted in pores becoming blocked. There was evidence of a guar gum residue that filled the majority of the inflow section (Figures 15, 16), causing the carbon content of the post-flow sample to be several times greater than that of the pre-flow sample. Kolb and Kamaria (1971) compared effects of guar gum gels on sandstones and limestones and found that guar gum has a greater effect on limestone porosity than sandstone porosity. However, Kolb and Kamaria (1971) do not examine if the limestone's lower porosity or different chemical composition ($CaCO_3$ vs. SiO_2) could be the cause of guar gum's unequal effects and conclude that additional research is needed to understand why limestone is more affected than sandstone.

Guar gum's presence appears to be accompanied by higher aluminum and potassium concentrations along with slightly lower silica contents in SEM-EDS elemental analysis and mapping of the inflow surface (Figures 15, 16, 17). The higher observed aluminum and potassium concentrations are likely the effect of the SEM's interaction volume including some clay minerals because the guar gum and quartz contain no aluminum or potassium; therefore, the correlation between carbon, aluminum, potassium, and silica contents suggests that the guar gum adheres preferentially to clay minerals. However, the Berea sandstone does not contain enough clay minerals to account for the percentage of the area covered by the guar gum on the inflow sample. As seen in SEM images, some of the grains have thin clay coatings that could help promote the guar gum to adhere to the surface, however the surface roughness of the angular quartz and detrital quartz within the pores may promote trapping of the guar gum.

SEM-EDS analysis also identified iron species, likely iron hydroxide or iron oxide that appear as lighter grains in SEM-BSE images (Figure 15), although the iron species are not a large modal component of the Berea sandstone. However, iron appears to be homogenously dispersed in the guar gum coating on the inflow surface (Figure 17). Guar Gum Spectra 1 in Figure 16 also contained trace concentrations of nickel, a common iron substitute. Some of the iron observed in the SEM-EDS analysis may be a product of secondary fluorescence from iron-oxide. Conversely, the trace concentrations of iron may be a product of using tap water to dissolve the guar gum for this experiment. Future iterations will use de-ionized water during the flow-through process to avoid this potential complication.

Abdulrahman and Alsewailem (2011) found that adding ~20 weight percent NaCl to a guar gum solution substantially increased viscosity. Although the sodium observed (<1 weight percent) is four orders of magnitude lower than in the Abdulrahman and Alsewailem (2011) study, the role NaCl plays in determining guar gum solution viscosity underlines the importance of using de-ionized water in future studies to avoid sodium contamination.

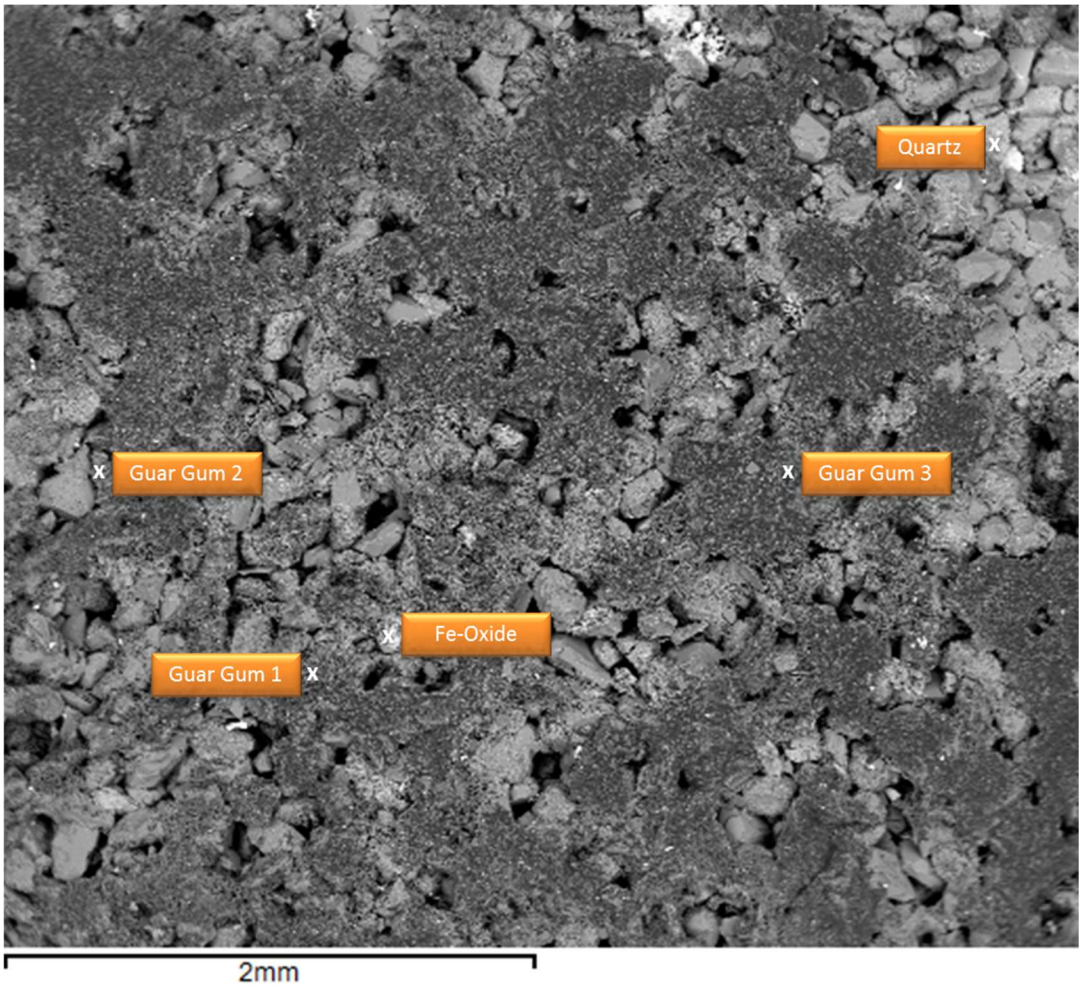

Spectra	C wt. %	O wt. %	Na wt. %	Mg wt. %	Al wt. %	Si wt. %	P wt. %	Cl wt. %	K wt. %	Ca wt. %	Ti wt. %	Fe wt. %
Guar Gum 1	23.29	53.06	BDL	BDL	23.02	0.34	0.08	BDL	BDL	0.02	0.13	0.07
Guar Gum 2 w/ Fe-Oxide	48.95	24.57	0.06	0.04	1.07	0.47	0.02	BDL	0.08	BDL	9.34	15.40
Quartz	6.21	53.78	BDL	BDL	BDL	40.01	BDL	BDL	BDL	BDL	BDL	BDL
Fe-Oxide	5.58	49.68	0.28	0.36	2.60	4.27	0.37	0.24	0.56	0.10	0.02	35.94

Figure 15: SEM-BSE image coupled with EDS of the Berea sandstone inflow section with a dark coating of guar gum.

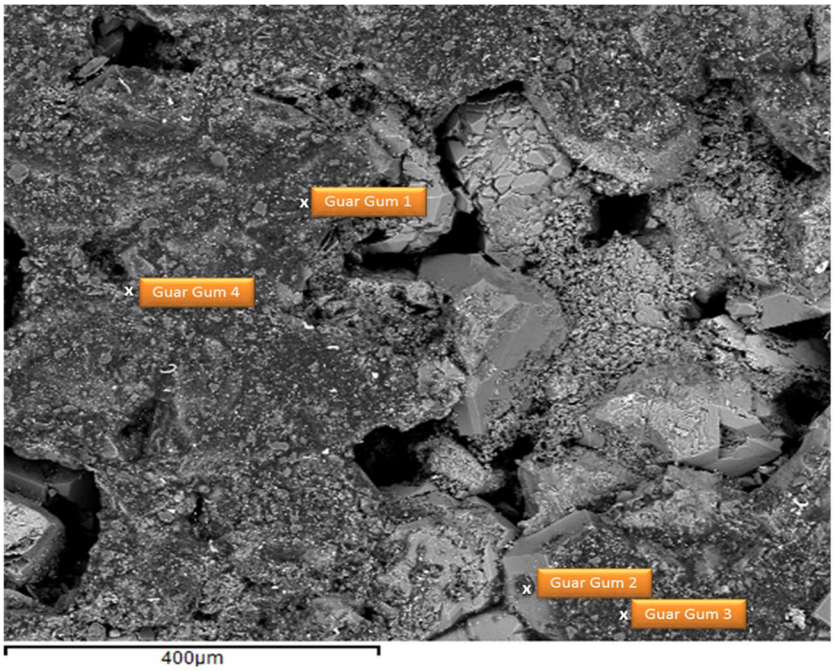

Spectra	C wt. %	O wt. %	Al wt. %	Si wt. %	P wt. %	Cl wt. %	K wt. %	Ca wt. %	Ti wt. %	Fe wt. %	Ni wt. %
Guar Gum 1	71.91	15.32	0.52	9.01	0.08	0.20	0.04	0.12	2.24	0.19	0.28
Guar Gum 2 w/ Fe-Oxide	27.38	34.39	1.00	9.44	BDL	BDL	BDL	BDL	4.31	23.49	BDL
Guar Gum 3	67.40	26.78	0.69	1.63	BDL	0.21	BDL	BDL	2.98	0.30	BDL
Guar Gum 4	60.02	37.99	BDL	1.99	BDL	BDL	BDL	BDL	BDL	BDL	BDL

Figure 16: SEM-BSE image and EDS analysis of the guar gum at the granular level. The guar gum does not appear to adhere as a thin coating across all minerals' surfaces. Instead, the guar gum prefers to stay in contiguous volumes within the Berea sandstone with areas of unblocked pore space and uncovered minerals.

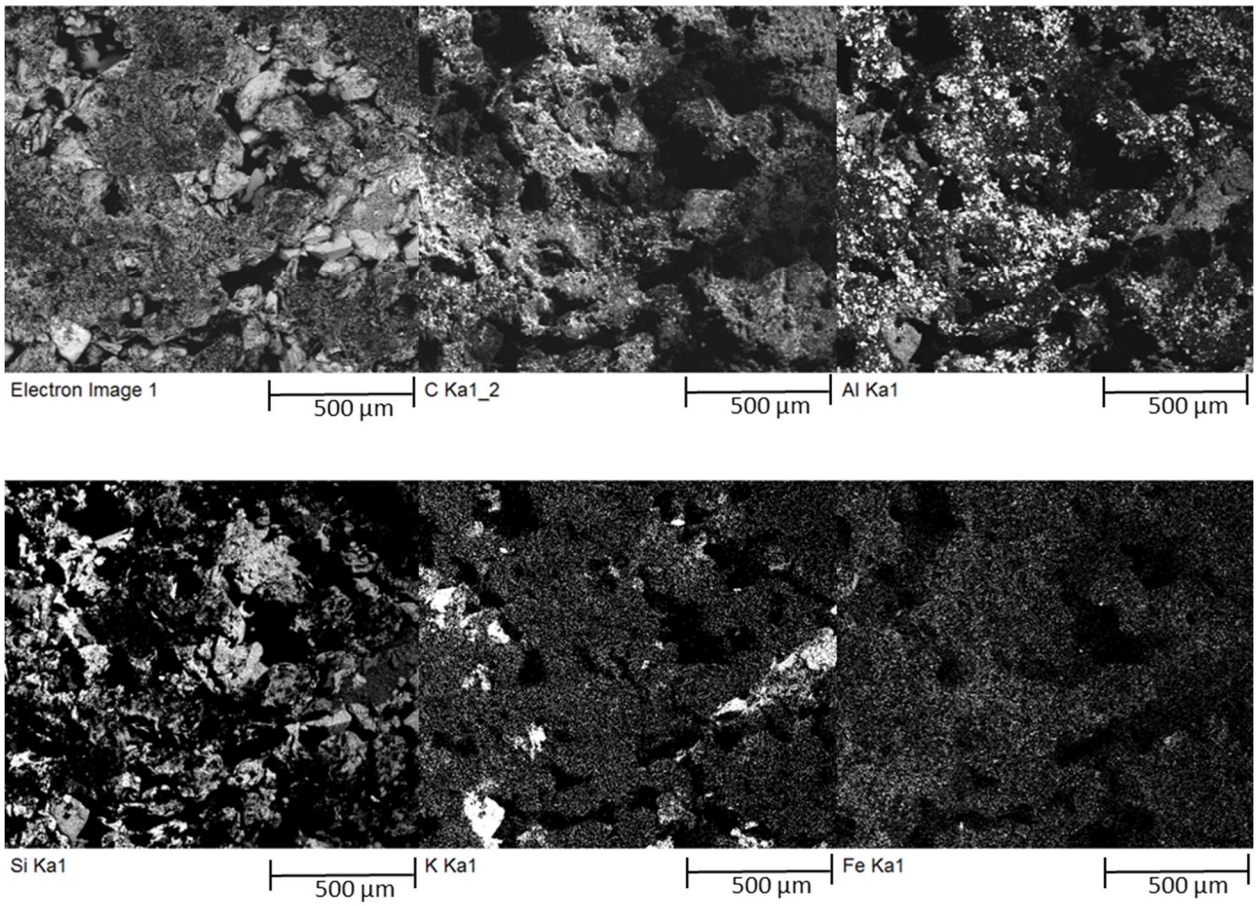

Figure 17: SEM-EDS elemental maps of Berea sandstone inflow surface. The detection of non-carbon elements through the guar gum coating suggests the guar gum layer is thin (<10 µm). Regions of higher carbon concentrations (guar gum) appear to be accompanied by aluminum, potassium, and lower silica concentrations, suggesting guar gum preferentially adheres to clay minerals. Each frame is of the same field of view.

3.2.2 Internal and Outflow: Berea-Guar Gum Flow-Through Analysis

Guar gum was mostly deposited in the pore space of the Berea sandstone within ~3 cm from the core's inflow surface, and the volume of the guar gum adhering to the sandstone appears to decrease with increasing distance from the inflow surface (Figure 14, 18). In Figure 18, the internal section of the Berea sandstone does not appear to be as filled with guar gum as the inflow sample surface. The guar gum invades some but not all pore spaces. This phenomenon may be attributed to the pores' interconnectivity and the guar gum's limited solubility in solution (Weaver et al., 2003; Kawamura, 2008). The insoluble particulates could block the inflow surface and restrict flow. As the guar gum moves through the sandstone, its abundance decreases with respect to that of the surrounding sandstone, suggesting limited transport of the material.

As the guar gum abundance decreases, organic particles of carbon and nitrogen become observable (Figure 19). These individual particles do not seem to be dependent on pore space. The carbon-nitrogen particles also appear on the outflow surface of the Berea core. Figure 20 gives the elemental composition of the carbon-nitrogen particles along with the composition for the surrounding Berea core outflow surface. Figure 20 also provides an elemental map displaying the composition of the organic particles surrounding Berea sandstone.

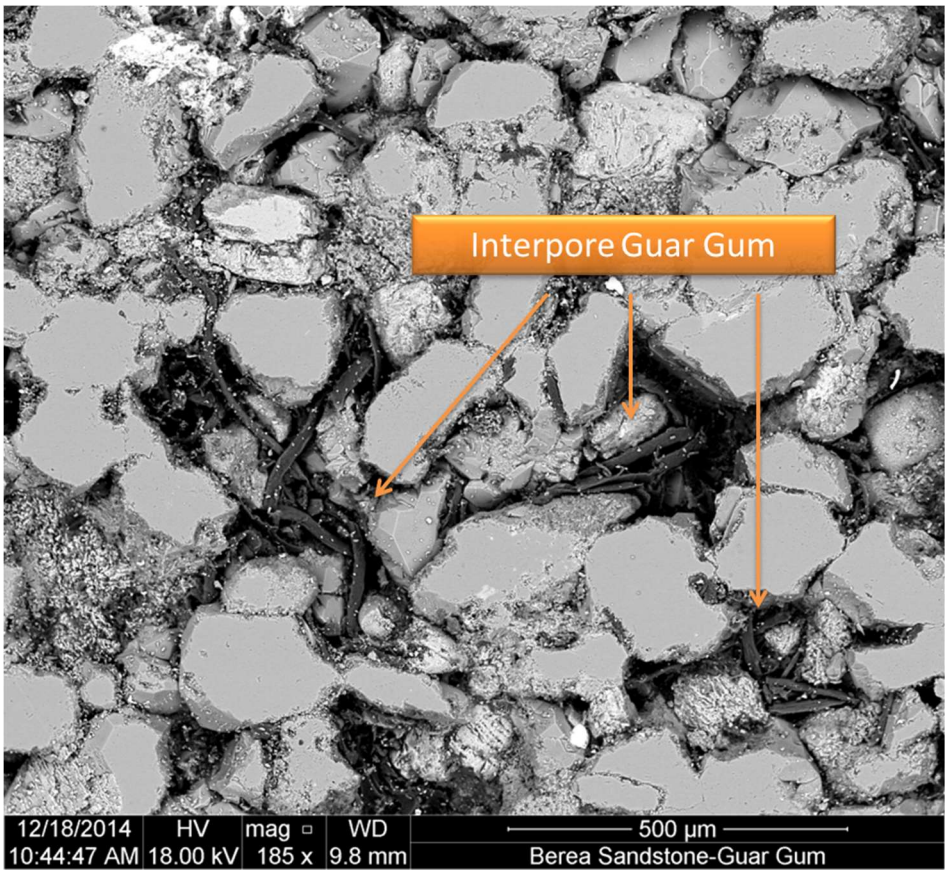

Figure 18: SEM-BSE image of guar gum filling pore spaces. This image is of a core cut ~6 cm from the inflow surface.

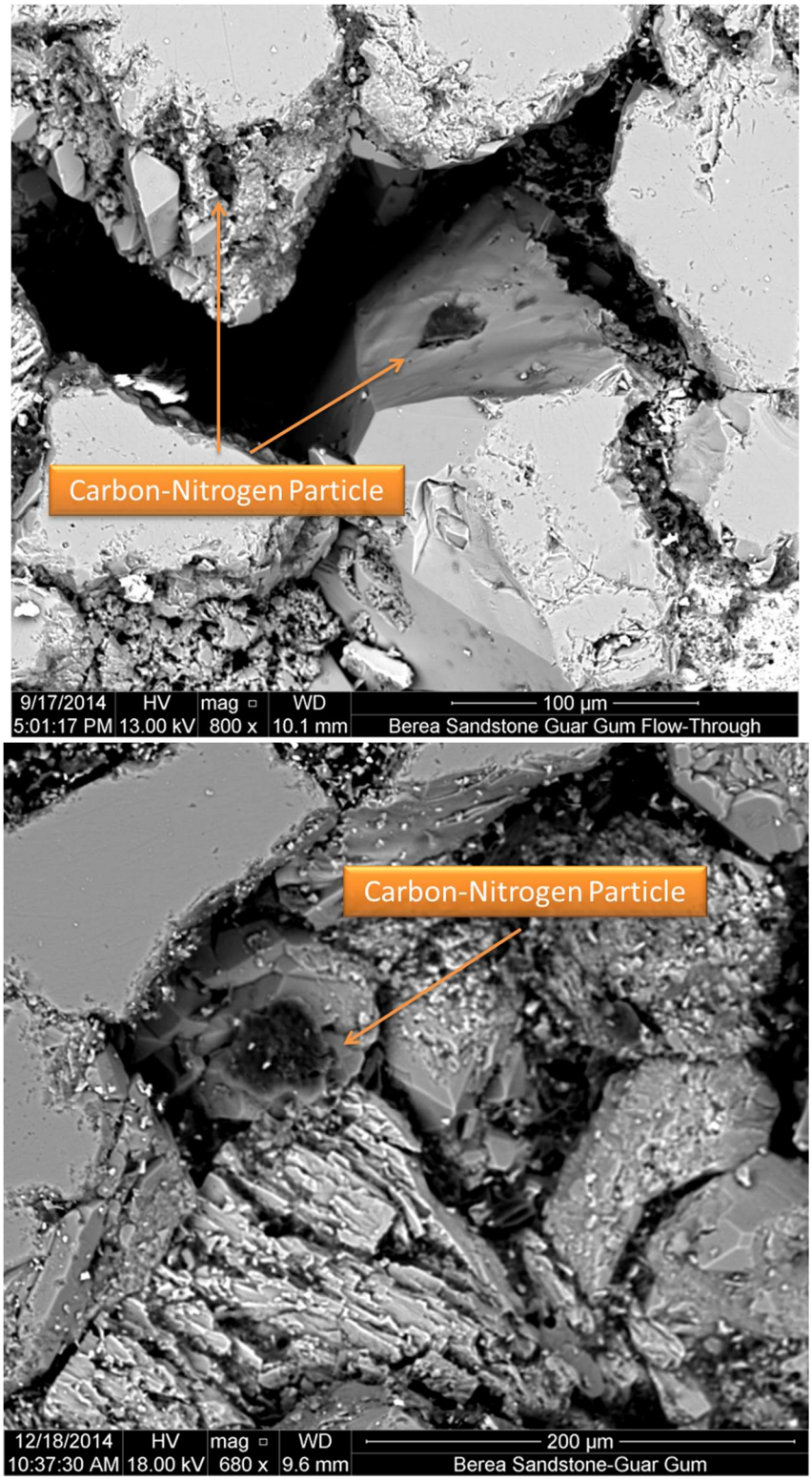

Figure 19: SEM-BSE image of organic carbon and nitrogen. These organic particles (depicted by darker objects in the images) were less than 6 cm from the inflow surface.

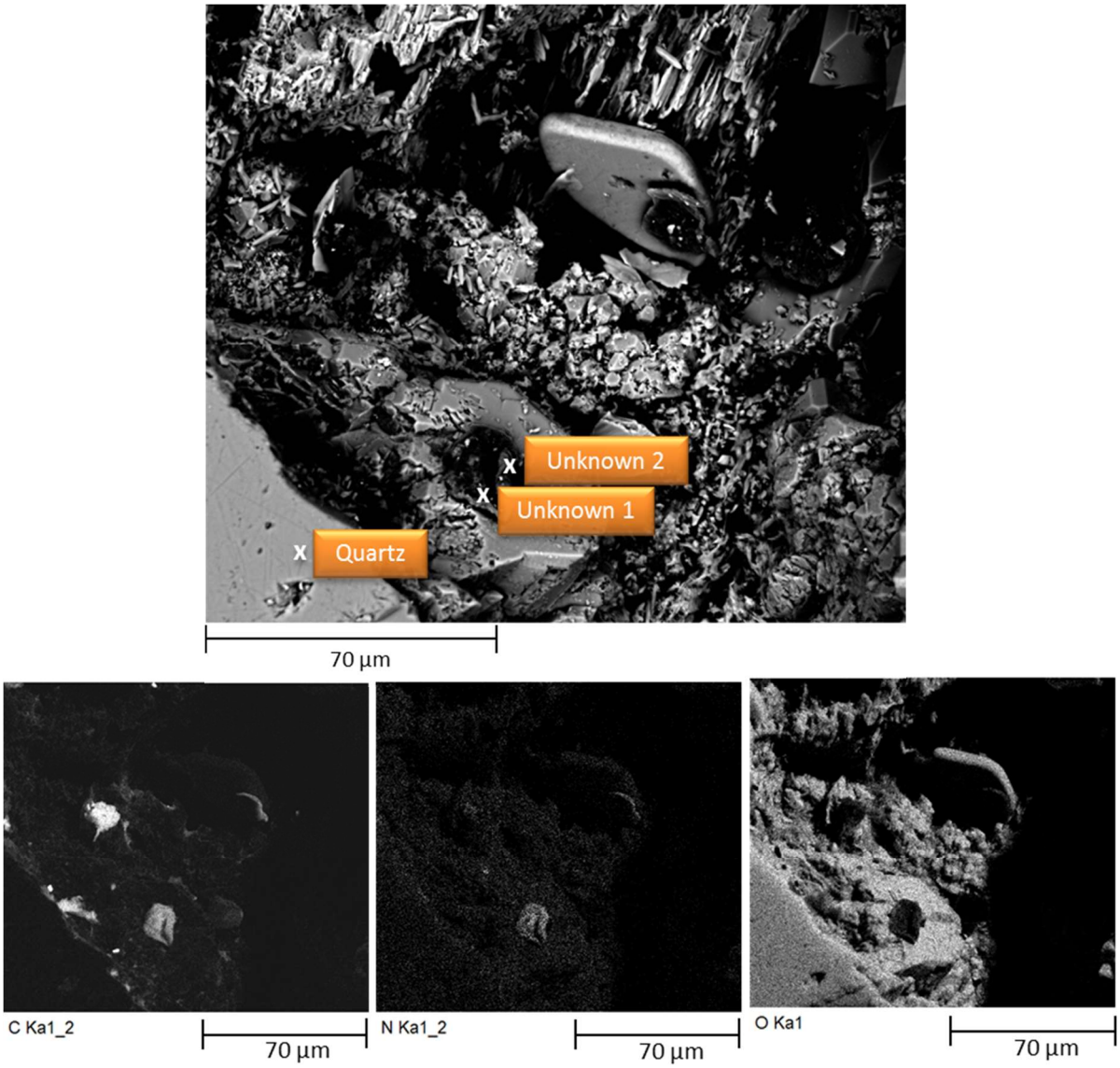

Spectra	C wt. %	N wt. %	O wt. %	Na wt. %	Al wt. %	Si wt. %	S wt. %	Cl wt. %	K wt. %	Fe wt. %
Unknown 1	48.92	21.10	23.34	1.67	0.09	2.89	1.42	BDL	BDL	0.58
Unknown 2	46.13	15.31	31.81	1.63	0.12	3.61	1.38	BDL	BDL	BDL
Quartz	2.64	BDL	58.50	BDL	BDL	38.58	BDL	BDL	BDL	BDL

Figure 20: SEM-BSE images and maps coupled with EDS analysis identify organic particles in Berea outflow sample.

Elemental maps depict the strong contrast of the compositions of the organic-rich carbon particles, against the Berea sandstone. The carbon-nitrogen particles appear relatively depleted of oxygen. The traces of sulfur, sodium, and aluminum in the carbon-nitrogen material suggest that some sort of sulfur, sodium, and aluminum species are present. The silica, which has greater concentrations than the sulfur, sodium, and aluminum, is likely a product of the SEM beam interaction volume including quartz, suggesting these less abundant elements could also be products of an interaction volume larger than the phase being analyzed.

The carbon-nitrogen particles may be a product of microbial activity fixing nitrogen from the air to organic products, or a contaminant from the Struers cooling fluid used to cut the samples. Previous microbial research does not indicate that microbes consume atmospheric nitrogen when in contact with guar gum (Salyers et al., 1977; Salyers et al., 1978; Hartemink et al., 1999). Mariotti et al. (2001) studied whether guar gum could affect the absorption of nitrogen in the digestive tracks of larger organisms and concluded that guar gum had no noticeable effect. Contamination from the Struers cooling fluid is a reasonable cause for observation of these particles. The C:N ratio appears to be roughly 2:1, and the lack of oxygen in the particles is consistent with the HCCN chemical composition of the Struers cooling fluid.

Fully understanding the complete geochemical implications of guar gum's interaction with the Berea sandstone requires additional research. This initial study shows that residual guar gum remains in contact with a sandstone after the fluid. Future research should utilize only different de-ionized water cutting techniques to remove the possibility of exposing samples to potential contaminants.

4. CONCLUSION

The Marcellus shale of the Appalachian Basin is undergoing hydraulic fracturing to promote natural gas production from the shale. Hydraulic fracturing fluid emplaces several chemicals into the deep subsurface to extract shale-gas. The degradation pathways and reactive potential of these chemicals with substrate mineralogy has not been widely reported in the existing literature. Should a spill of these hydraulic fracturing fluids occur, the necessary environmental remediation methods and residence time of these chemicals in the environment need to be known in order to implement the appropriate environmental management strategies.

This report describes minerals in the Oriskany and Berea sandstones and the Marcellus shale (e.g. quartz, feldspar, calcium carbonates, halite, kaolinite, illite, chlorite, mica, pyrite, tourmaline, zircon, siderite, gypsum, and anhydrite). This study reviewed common hydraulic fracturing fluid organic chemical additives and summarized their degradation pathways and reactive potential with substrate mineralogy of several of the more common hydraulic fracturing organic chemical additives (polyacrylamide, ethylene glycol, poly[diallyldimethylammonium chloride], glutaraldehyde, and isopropanol). The range of degradation variables is as diverse as the number of hydraulic fracturing fluids used in the industry. Every spill will need to be addressed on a case-by-case basis to account for fracturing fluids specific to that spill.

Berea sandstone exposed to guar gum was characterized and analyzed in a water solution. The first several centimeters of the Berea sandstone was partially coated and filled in by a thin layer of guar gum; however, the guar gum residue did not penetrate deeply into the sample.

5. REFERENCES

Abdulrahman, A. A.; Alsewailem, F. D. *Adsorption of Guar, Xanthan and Xanthan-Guar Mixtures on High Salinity, High Temperature Reservoirs*, Offshore Mediterranean Conference and Exhibition, Ravenna, Italy, March 23–25, 2011; Offshore Mediterranean Conference: Ravenna, 2011.

Berner, R. A. The role of magnesium in the crystal growth of calcite and aragonite from sea water. *Geochimica Et Cosmochimica Acta* **1975,** *39*, 489–504.

Bjelopavlic, M.; Singh, P. K.; El-Shall, H.; Moudgil, B. M. Role of Surface Molecular Architecture and Energetics of Hydrogen Bonding Sites in Adsorption of Polymers and Surfactants. *Journal of Colloid and Interface Science* **2000,** *226*, 159–169.

Blauch, M. E.; Meyers, R. R.; Lipinski, B. A.; Houston, N. A. *Marcellus Shale Post-Frac Flowback Waters—Where is All That Salt Coming From and What are the Implications?* Society of Petroleum Engineers Eastern Regional Meeting, Charleston, WV, Sept 23–25, 2009; Society of Petroleum Engineers: Charleston, WV.

Boulton, A.; Fornasiero, D.; Ralston, J. Selective Depression of Pyrite with Polyacrylamide Polymers. *International Journal of Mineral Processing* **2000,** *61*, 13–22.

Boyce, M. L.; Carr, T. R. *Lithostratigraphy and Petrophysics of the Devonian Marcellus Interval in West Virginia and Southerwestern Pennsylvania Abstract*, American Association of Petroleum Geologists Student Expo, Sept 21–22, 2009.

Bruner, K. R.; Smosna, R. *A Comparative Study of the Mississippian Barnett Shale, Forth Worth Basin, and Devonian Marcellus Shale, Appalachian Basin*; DOE/NETL-2011/1478; National Energy Technology Laboratory: Morgantown, WV, 2011.

Bustard, M.; Meeyo, V.; Wright, P. C. Biodegradation of Isopropanol in a Three-Phase Fixed Bed Bioreactor: Start Up and Acclimation Using a Previously Enriched Microbial Culture. *Environmental Technology* **2001,** *22*, 1193–1201.

Capo, R. C.; Stewart, B. W.; Rowan, E. L; Kolesar, C. A.; Wall, A. J.; Chapman, E. C.; Hammack, R. W.; Schroeder, K. T. The Strontium Isotopic Evolution of Marcellus Formation Produced Waters, Southwestern Pennsylvania. *International Journal of Coal Geology* **2014,** *126*, 57–63.

Chapman, E. C.; Capo, R. C.; Stewart, B. W.; Kirby, C. S.; Hammack, R. W.; Schroeder, K. T.; Edenborn, H. M. Geochemical and Strontium Isotope Characterization of Produced Waters from Marcellus Shale Natural Gas Extraction. *Environmental Science and Technology* **2012,** *46*, 3545–3553.

Dana, J. D. *Manual of Science*, 23rd ed.; Klein, C., Dutrow, B., Eds.; John Wiley and Sons: New Jersey, 2008.

de Ory, I.; Romero, L. E.; Cantero, D. Modeling the Kinetics of Growth of the *Acebactor Aceti* in Discontinuous Culture: Influence of the Temperature of Operation. *Applied Microbiology Biotechnology* **1998,** *49*, 189–193.

Deer, W. A.; Howie, R. A.; Zussman, J. *An Introduction to the Rock Forming Minerals,* 2nd ed.; Pearson Education Limited: Harlow, 1992.

Dresel, P. E.; Rose, A. W. *Chemistry and origin of oil and gas well brines in western Pennsylvania*; Open-File Report OFOG 10–01.0; Pennsylvania Geological Survey, 4th series, 2010.

Dwyer, D. F.; Tiedje, J. M. Metabolism of Polyethylene Glycol by Two Anaerobic Bacteria, *Desulfovibrio Desulfuricans* and a *Baceroides sp*. *Applied and Environmental Microbiology* **1986,** *52*, 852–856.

Edwards, N.; Lowry, G.; Karamalidis, A. K. Hydrolysis of Hydraulic Fracturing Fluid Organic Additives and Their Interaction with Pyrite, National Groundwater Association Workshop, Pittsburgh, PA, Nov 13–14, 2014; National Groundwater Association: Westerville, OH, 2014.

Emmanuel, E.; Hanna, K.; Bazin, C.; Keck, G.; Clement, B.; Perrodin, Y. Fate of Glutaraldehyde in Hospital Wastewater and Combined Effects of Glutaraldehyde on Surfactants on Aquatic Organisms. *Environmental International* **2005,** *31*, 399–406.

Enomoto, C. B.; Coleman, J. L.; Haynes, J. T.; Whitmeyer, S. J.; McDowell, R. R.; Lewis, E. J. *Geology of the Devonian Marcellus Shale—Valley and Ridge Province, Virginia and West Virginia— A Field Trip Guidebook,* The American Association of Petroleum Geologists Eastern Section Meeting, Sept 28–29, 2011; American Association of Petroleum Geologists.

Flaten, E. M. Polymorphism and Morphology of Calcium Carbonate Precipitated in Mixed Solvents of Ethylene Glycol and Water. *Journal of Crystal Growth* **2009,** *311*, 3533–3538.

Flaten, E. M.; Seiersten, M.; Andreassen, J. P. Induction Time Studies of Calcium Carbonate in Ethylene Glycol and Water. *Chemical Engineering Research and Design* **2010,** *88*, 1659–1668.

Fox, P.; Ketha, S. Anaerobic Treatment of High-Sulphate Wastewater and Substrate Interactions with Isopropanol. *Journal of Environmental Engineering* **1996,** *122*, 989–994.

Frac Focus. What Chemicals are Used. https://fracfocus.org/chemical-use/what-chemicals-are-used (accessed Feb 20th, 2015).

Gastone, F.; Tosco, T.; Sethi, R. Guar Gum Solutions for Improved Delivery of Iron Particles in Porous Media (Part 1): Porous Medium Rheology and Guar Gum-Induced Clogging. *Journal of Contaminant Hydrology* **2014,** *166*, 23–33.

Graveling, G. J.; Ragnarsdottir, V. K.; Allen, G. C.; Eastman, J.; Brady, P. V.; Basley, S. D. Controls on Polyacrylamide Adsorption to Quartz, Kaolinite, and Feldspar. *Geochimicia et Cosmochimica Acta* **1990,** *61*, 3515–3523.

Gruden, C. L.; Dow, S. M.; Hernandez, M. T. Fate and Toxicity of Aircraft Deicing Fluid Additives through Anaerobic Digestion. *Water Environment Research* **2001,** *73*, 72–79.

Guevellou, Y.; Noik, C.; Lecourtier, J.; Defives, D. Polyacrylamidc Adsorption onto Dissolving Minerals at Basic pH. *Colloids and Surfaces A: Physiochemical and Engineering Prospects* **1995,** *100*, 173–185.

Hartemink, R.; Schoustra, S. E.; Rombouts, F. M. Degradation of Guar Gum by Intestinal Bacteria. *Bioscience Microflora* **1999,** *18*, 17–25.

Hayduk, W.; Malik, V. K. Density, Viscosity, and Carbon Dioxide Solubility and Diffusivity in Aqueous Ethlyene Glycol Solutions. *Journal of Chemical Engineering* **1971,** *16*, 143–146.

Heinrich, E. W. M. Geologic Types of Glass-sand Deposits and some North American Representatives. *The Geological Society of America Bulletin* **1981,** *92*, 611–613.

Hosterman, J. W.; Whitlow, S. I.; Clay Mineralogy of Devonian Shales in the Appalachian Basin. Geological Survey Professional Paper 1298: U.S. Geological Survey, 1983.

Huang, Y. L.; Li, Q. B.; Deng, X.; Lu, Y. H.; Liao, X. K.; Hong, M. Y.; Aerobic and Anaerobic Biodegradation of Polyethlyene Glycols Using Sludge Microbes. *Process Biochemistry*, **2005,** *40*, 207–211.

Hwang, Y.; Sakuma, H.; Tanaka, T. Denitrification with Isopropanol as a Carbon Source in a Biofilm System. *Water Science Technology* **1995,** *30*, 69–81.

Inoue, A.; Horikoshi, K. A. Pseudomonas Thrives in High Concentrations of Toleuene. *Nature* **1989,** *388*, 264–266.

Jagucki, M.; Darner, R. A. Ground-Water Quality in Geauga County, Ohio—Review of Previous Studies, Status in 1999, a Comparison of 1986 and 1999 Data. Report 01-416: Water–Resources Investigations, 2001.

John, W. Synthesis, Properties, and Analysis of Polydadmac for Water Purification. Ph.D. Dissertation, Stellenbosch University, Stellenbosch, South Africa, 2008.

Kahrilas, A.; Blotevogel, J.; Stewart, P. S.; Borch, T. Biocides in Hydraulic Fracturing Fluids: A Critical Review of Their Usage, Mobility, Degradation, and Toxicity. *Environmental Science and Technology* **2015,** *49*, 16–32.

Kanemitu, H.; Fukuda, M.; Yano, K. Plasmid-Borne Biodegradation of Toluene and Ethylbenzene in a Pseodomonas. *Journal of Fermentation Technology* **1980,** *57*, 175–181.

Kay-Shoemake, J. L.; Watwood, M. E.; Lentz, R. D.; Sojka, R. E. Polyacrylamide as an Organic Nitrogen Source for Soil Microorganisms with Potential Effects on Inorganic Soil Nitrogen in Agricultural Soil. *Soil Biol. Biochemistry* **1998,** *30*, 1045–1052.

Kawamura, Y. *Guar Gum Technical and Chemical Assessment*. Joint FAO/WHO Expert Committee on Food Additives; Rome, Italy, 2008.

Kolb, A. K.; Kamaria, P. *Laboratory Investigation of Damage from Guar Gum Base Gels*, Society of Petroleum Engineers Eastern Regional Meeting, Nov 4–5, 1971; Society of Petroleum Engineers: Charleston, WV, 1971.

Konopacka-Łyskawa, D.; Lackowski, M. Influence of Ethylene Glycol on $CaCO_3$ Particles Formation via Carbonation in the Gas–Slurry System. *Journal of Crystal Growth* **2011,** *321*, 136–141.

Kostelnik, K.; Carter, K. M. Unraveling the Stratigraphy of the Oriskany Sandstone: A Necessity in Assessing Its Site-Specific Carbon Sequestration Potential. *Environmental Geosciences* **2009,** *16*, 187–200.

Landrum, P. F.; Sano, L.; Mapili, M. A.; Garcia, E.; Krueger, A. M.; Russell, A. M. *Degradation of Chemical Biocides with Application to Ballast Water Treatment*; GLERL-123; NOAA Technical Memorandum, 2003.

Laughrey, C. D.; Ruble, T. E.; Lemmens, H.; Kostelnik, J.; Butcher, A. R.; Walker, G. *Black Shale Diagenesis: Insights from Integrated High-Definition Analyses of Post-Mature Marcellus Presentation*, American Association of Petroleum Geologists Annual Convention, Houston, TX, June 23, 2011; American Association of Petroleum Geologists.

Lecourtier, J.; Lee, L. T.; Chauveteau, G. Adsorption of Polyacrylamides on Siliceous Minerals, *Colloids and Surfaces* **1990,** *47*, 219–231.

Leff, E. *Supplemental Generic Environmental Impact Statement on the Oil, Gas, and Mining Regulatory Program;* New York State Department of Environmental Conservation: Albany, NY, 2011.

Leung, H. W. Ecotoxicology of Glutaraldehyde: Review of Environmental Fate and Effects Studies. *Ecotoxicology and Environmental Safety* **2001a,** *49*, 26–39.

Leung, H. W. Aerobic and Anaerobic Metabolism of Glutaraldehyde in a River Water–Sediment System. *Archives of Environmental Contamination and Toxicology* **2001b,** *41*, 267–273.

Mahajan, V.; Misra, M.; Zhong, K.; Fuerstenau, M. C. Enhanced Leaching of Copper from Chalcopyrite in Hydrogen Peroxide–Glycol System. *Minerals Engineering* **2007,** *20*, 670–674.

Mali, Y. N.; Pawar, S. P.; Gujarathi, N. A.; Rane, B. R.; Bakliwal, S. R.; Applications of Natural Polymers in Sustained Release Drug Deliversy System: A Review. *Pharma Science Monitor* **2012,** *3*, 3314–3335.

Mariotti, F.; Pueyo, M. E.; Tome, D.; Benamouzig, R.; Mahe, S. Guar Gum Does Not Impair the Absorption and Utilization of Dietary Nitrogen but Affects Early Endogoneous Urea Kinetics in Humans. *American Journal of Clinic Nutrition* **2001,** *74*, 487–493.

McCarthy, K.; Rojas, K.; Niemann, M.; Palmowski, D.; Peters, K.; Stankiewicz, A. Basic Petroleum Geochemistry for Sour Rock Evaluation. *Oil Field Review* **2011,** *23*, 32–43.

Midwest Regional Carbon Sequestration Partnership. MRCSP Regional Geologic Cross Section and Correlation Chart. http://www.mrcsp.org/ (accessed Feb 17, 2015).

Moriya, K; Horikoshi, K. Isolation of a Benzene-Tolerant Bacterium and Its Hydrocarbon Degradation. *Journal of Fermentation Bioengineering* **1993,** *76*, 397–399.

Morrison, R. T.; Boyd, R. N. *Organic Chemistry*, 5th ed.; Allyn Bacon: New York, 1987.

Murrays, J.; Roberta, A.; Hall, A.; Griffini, M. Microbial Metabolism by a Pure Strain of *Psuedomonas sp*. *Journal of General Microbiology* **1980,** *120*, 89–94.

Nakamiya, K.; Kinoshita, S. Isolation of Polyacrylamide-Degrading Bacteria. *Journal of Fermentation* **1995,** *80*, 418–420.

Nasser, M. S.; James, A. E. Effect of Polyacrylamide Polymers on Flox Size and Rheological Behavior of Kaolinite Suspensions. *Colloids and Surfaces A: Physiochemical and Engineering Aspects* **2007,** *301*, 311–322.

Nesse, W. D. *Introduction to Mineralogy*, 2nd ed.; Oxford University Press: Oxford, New York: 2012.

Nyahay, R.; Leone, J.; Smith, L. B.; Martin, J. P.; Jarvie, D. J. *Update on Regional Assessment of Gas Potential in the Devonian Marcellus and Ordovician Utica Shales of New York,* American Association of Petroleum Geologists Eastern Section Meeting, Lexington, KY, Sept 16–18, 2007; American Association of Petroleum Geologists Reservoir Characterization Group, New York.

Peng, P.; Garnier, G. Effect of Cationic Polyacrylamide on Precipitated Calcium Carbonate Flocculation: Kinetics, Charge Density, and Ionic Strength. *Colloids and Surfaces A: Physiochemical and Engineering Aspects* **2012,** *408*, 32–39.

Pepper, J. F.; De Witt, W. J.; Demareset, D. F. *Geology of the Bedford Shale and Berea Sandstone in the Appalachian Basin: A Study of the Stratigraphy, Sedimentation, and Paleogeography of Rocks of Bedford and Berea Age in Ohio and Adjacent States*; U.S. Department of the Interior and the U.S. Geological Survey: 1954.

Perkins, D. *Mineralogy*, 3rd ed.; Folchetti, N., Ed.; Pearson Education: Upper Saddle River, NJ, 2011.

Poppe, L. J.; Paskevich, V. F.; Hathaway, J. C.; Blackwood, D. S. *USGS Coastal and Marine Geology Program*; Open-File Report 01-041; U.S. Geoloical Survey: 2002.

Quinlan, C.; Strevett, K.; Ketcham, M. VOC Elimination in a Compost Biofilter Using Previously Acclimated Bacterial Inoculum. *Journal of the Air Waste Management Association* **1999,** *49*, 544–553.

Repetski, J. E.; Ryder, R. T.; Weary, D. J.; Harris, A. G.; Trippi, M. H. Thermal Maturity Patterns (CAI and %R0) in Upper Ordovician and Devonian Rocks of the Appalachian Basin: A Major Revision of USGS Map I-917-E Using New Subsurface Collections; Scientific Investigations Map 3006; U.S. Geological Survey, Reston, VA, 2008.

Rowan, E. L. *Burial and Thermal History of the Central Appalachian Basin, Based on Three 2-D Models of Ohio, Pennsylvania, and West Virginia*; Open-File Report 2006-1019; U.S. Geological Survey, Reston, VA, 2006.

Sageman, B. B.; Murphy, A. E.; Werne, J. P.; Ver Straeten, C. A.; Hollander, D. J.; Lyons, T. W. (2003). A Tale of Shales: The Relative Roles of Production, Decomposition, and Dilution in the Accumulation of Organic-Rich Strata, Middle-Upper Devonian, Appalachian Basin. *Chemical Geology* **2003,** *195*, 229–273.

Salyers, A. A.; Palmer, J. K.; Wilkens, T. D. Degradation of Polysaccarides by Intestinal Bacterial Enzymes. *The American Journal of Clinical Nutrition* **1978**, *31*, 319–322.

Salyers, A. A.; Vercellotti, J. R.; West, S. H.; Wilkins, T. D. Fermentation of Mucin and Plant Polysaccarides by Strains of Bacteroides from the Human Colon. *Applied and Environmental Microbiology* **1977,** 319–322.

Samoshina, Y.; Diaz, A.; Becker, Y.; Nylander, T.; Lindman, B. Adsorption of Cationic, Anionic, and Hydrophobically Modified Polyacrylamides on Silica Surfaces. *Colloids and Surfaces A: Physiochem. Eng. Aspects* **2003,** *231*, 195–205.

Schramm, E.; Schink, B. Ether-Cleaving Enzyme and Diol Dehydratase Involved in Anaerobic Polyethylene Glycol Degradation by a New Homoacetogenic Bacterium. *Biodegradation*, **1991,** *2*, 71–79.

Selley, R. C. *Elements of Petroleum Geology*, 2nd ed.; Academic Press: San Diego, CA, 1997.

Siegel, J. M.; Kamen, M. D. Studies on the Metabolism of Photosynthetic Bacteria. VI. Metabolism of Isopropanol by a New Strain of *Rhodopseudomanas Gelatinosa*. *Journal of Bacteriology* **1950,** *4*, 286–293.

Soeder, D. L. Porosity and Permeability of Eastern Devonian Gas Shale. *Society of Petroleum Engineers Formation Evaluation* **1988,** *3*, 116–124.

Soeder, D. J.; Enomoto, C. B.; Chermak, J. A. The Devonian Marcellus Shale and Millboro Shale. *The Geological Society of America Field Guide* **2014,** *35*, 129–160.

Stahl, J. D.; Cameron, M. D.; Haselbach, J.; Aust, S. D. Biodegradation of Superabsorbent Polymers in Soil. *Environmental Science and Pollution* **2000,** *7*, 83–88.

Tekin, N.; Demirbas, O.; Alkan, M. Adsorption of Cationic Polyacrylamide onto Kaolinite. *Microporous and Mesoporous Materials* **2005,** *85*, 340–350.

Ueyama, H.; Yamauti, Y.; Tuki, N.; Fukibama, T. Studies on the Fermentation of Petrochemicals. I. Taxonomic studies on *Arthobacter sp*. isolated from soil. *Journal of Fermentation Technology* **1971,** *49*, 581–586.

U.S. Geological Survey. Natural Attenuation. http://toxics.usgs.gov/definitions/natural_attenuation.html (accessed Feb 17, 2015).

Veltman, S.; Schoenberg, T.; Switzenbaum, M. S. Alcohol and Acid Formation During the Anaerobic Decomposition of Propylene Glycol under Methanogenic Conditions. *Biodegradation* **1998,** *9*, 113–118.

Wallace, G. A.; Wallace, A. Control of Soil Erosion by Polymeric Soil Conditioners. *Soil Science* **1986,** *141*, 363–367.

Walter, L. M. Relative efficiency of carbonate dissolution and precipitation during diagenesis: a progress report on the role of solution chemistry. Roles of organic matter in mineral diagenesis. *Society of Economic Paleontologists and Mineralogists. Special Publication* **1986,** *38*, 1–12.

Wang, C. C.; Lee, C. M. Denitifrication with Acrylamide by Pure Culture of Bacteria Isolated from Acrylonitrile-Butadiene-Styene Resin Manufactured Wastewater Treatment System. *Chemosphere* **2001,** *44*, 1047–1053.

Wang, C.; Zhao, J.; Zhao, X.; Bala, H.; Wang, Z. Synthesis of Nanosized Calcium Carbonate (Aragonite) via Polyacrylamide Inducing Process. *Powder Technology* **2006,** *163*, 134–138.

Wang, D.; Wu, M.; Wang, Q.; Wang, T.; Chen, J. Controlled growth of uniform nanoflakes-built pyrite FeS_2 microspheres and their electrochemical properties. *Ionics* **2011,** *17*, 163–167.

Wang, G.; Carr, T. R. Organic-Rich Marcellus Shale Lithofacies Modeling and Distribution Pattern Analysis in the Appalachian Basin. *American Association of Petroleum Geologists Bulletin* **2013,** *97*, 2173–2205.

Weaver, J.; Gdanski, R.; Karcher, A. Guar Gum Degradation: A Kinetic Study, International Symposium on Oilfield Chemistry, Houston, Texas, Feb 5–7, 2003; Richardson: Society of Petroleum Engineers.

Wen, Q.; Chen, Z.; Zhao, Y.; Zhang, H.; Feng, Y. Biodegradation of Polyacrylamide by Bacteria Isolated from Activated Sludge and Oil-Contaminated Soil. *Journal of Hazardous Materials* **2010,** *175*, 955–959.

Werne, J. P.; Sageman, B. B.; Lyons, T. W.; Hollander, D. J. An Integrated Assessment of a "Type Euxinic" Deposit: Evidence for Multiple Controls on Black Shale Deposition in the Middle Devonian Oatka Creek Formation. *American Journal of Science* **2002,** *302*, 110–143.

Woodrow, D. L. Paleogeography, Paleoclimate, and Sedimentary Processes of the Late Devonian Catskill Delta. *Geological Society of America Special Paper* **1985,** *201*, 51–64.

Yen, T. F.; Chilingarian, G.V. *Developments in Petroleum Science: Oil Shale*; American Elsevier Publishing Company, Inc.: New York, 1976.

Zielinksi, R. E.; McIver, R. D. *Resource Exploration Assessment of the Oil and Gas Potential in Devonian Gas Shales in the Appalachian Basin*; MLM-MU-82-61-0002/DOE/DP/0053-1125; U.S. Department of Energy, Morgantown, WV, 1981.

Ziemkiewicz, P.; Hause, J.; Gutta, B.; Fillhart, J.; Mack, B.; O'Neil, M. *Final Report Water Quality Literature Review and Field Monitoring of Active Shale Gas Wells Phase I For "Assessing Environmental Impacts of Horizontal Gas Well Drilling Operations"*; West Virginia Department of Environmental Protection, Charleston, WV, 2013.

This page intentionally left blank.

Sean Plasynski
Executive Director
Technology Development & Integration Center
National Energy Technology Laboratory
U.S. Department of Energy

Jared Ciferno
Associate Director
Oil and Gas
Technology Development & Integration Center
National Energy Technology Laboratory
U.S. Department of Energy

Elena Melchert
Director
Division of Upstream Oil and Gas Research
U.S. Department of Energy

Cynthia Powell
Executive Director
Research & Innovation Center
National Energy Technology Laboratory
U.S. Department of Energy